National Oceanography Centre
NATURAL ENVIRONMENT RESEARCH COUNCIL

ESA Support to Science Element (STSE)
Cryosat+: Ocean Theme

ESA AO/1-6827/11/I-NB

CP4O – Cryosat Plus 4 Oceans
WP4000 Product Development and Validation

SAR Altimetry over the Open Ocean & the Coastal Zone

Product Validation Report (PVR)

Christine Gommenginger, Paolo Cipollini & Helen Snaith

National Oceanography Centre

23 June 2014

Version 1.0

National Oceanography Centre, Southampton
European Way, Southampton
SO14 3ZH, United Kingdom
Tel: +44 (0)23 80596413 Fax: +44 (0)23 80596400

DOCUMENT SIGNATURE TABLE

	Name	Institution	Signature	Date
Prepared by	C. Gommenginger, P. Cipollini	NOC		23/06/2014
Verified by				
Authorised by				

DISSEMINATION

To:	Copies	Means
Jérôme Benveniste	1	Jerome.Benveniste@esa.int
Salvatore Dinardo	1	Salvatore.Dinardo@esa.int
David Cotton	1	d.cotton@satoc.eu

ISSUE RECORD

Issue No.	Issue Date	Sections affected	Relevant information
1.0	23/06/2014	All	First issue

REFERENCE DOCUMENTS AND APPLICABLE DOCUMENTS

[RD1] Boy, F. & Moreau, T., 2013: Algorithm Theoretical Basis Document (ATBD) of the CPP SAR numerical retracker for oceans. CNES report reference S3A-NT-SRAL-00099-CNES, Version 1.0, 15/06/2013, 16 pp.

[RD2] Dinardo, S., 2014: GPOD CryoSat-2 SARvatore Software Prototype User Manual, Available from https://wiki.services.eoportal.org/tiki-index.php?page=GPOD+CryoSat-2+SARvatore+Software+Prototype+User+Manual

[RD3] Dinardo, S., 2013: Guidelines for the SAR (Delay-Doppler) L1b Processing. ESRIN report reference XCRY-GSEG-EOPS-TN-14-0042, Issue 2, Revision 3, 29/05/2013. Available from http://wiki.services.eoportal.org/tiki-download_wiki_attachment.php?attId=2540

[RD4] Ray, C., Martin-Puig, C., Clarizia, M-P, Ruffini, G., Dinardo, S., Gommenginger, C.P. & Benveniste, J., 2014: SAR Altimeter Backscattered Waveform Model, IEEE Trans. GeoSc. Remote Sensing, Accepted.

[RD5] Passaro, M., Cipollini, P., Vignudelli, S., Quartly, G.D. and Snaith, H.M., “ALES: a multi-mission adaptive sub-waveform retracker for coastal and open ocean altimetry”, *Remote Sensing of Environment*, Volume 145, 5 April 2014, Pages 173–189, http://dx.doi.org/10.1016/j.rse.2014.02.008

TABLE OF CONTENTS

1 PURPOSE OF THIS DOCUMENT

This document represents deliverable D4.2 “Product Validation Report” of WP4000 for the “SAR Altimetry over the Open Ocean and the Coastal Zone” sub-themes.

It reports the results of validation activities with Cryosat-2 SAR data that seek to determine the optimal methodology to retrack Cryosat-2 SAR L1B waveforms to retrieve Level 2 ocean geophysical parameters in the open ocean and the coastal zone. Two main approaches are considered:

- The CNES numerical retracking approach, documented in [RD1]
- The SAMOSA analytical retracking approach, documented in [RD2] and [RD4].

2 OBJECTIVES AND APPROACH

The main objectives of the validation activities are:

- to analyse Cryosat-2 Level 2 SAR retracked parameters for various L2 processing choices.
- to evaluate the Cryosat-2 Level 2 SAR retracked parameters against independent measurements from in situ sources and other satellites.

Objective 1 is addressed with Cryosat-2 SAR L2 products developed for various L2 SAR retracking choices and provided to the CP4O team by CNES and ESRIN.

For the most part, the L2 retracking was applied to Cryosat-2 L1B SAR waveforms obtained from the CNES Cryosat Prototype Products (aka “CPP”). The decision to use primarily CNES CPP products instead of Cryosat-2 operational products from ESA was taken after it became clear that operational ESA Cryosat-2 L1B SAR products (the “Kiruna” data) are optimised for sea ice applications, at the detriment of performance of SAR mode over water surfaces. One exception is the dataset (R5) provided by ESRIN based on their in-house L1B processing starting from C2 FBR.

Objective 2 is addressed by comparing the L2 SAR ocean parameters against measurements from buoys, tide gauges and other satellites. The validation focuses on Sea Surface Height (SSH), Significant Wave Height (SWH) and Received Power (Pu), linked to the Normalised Radar Cross Section (Sigma0).

3 DEVELOPMENT CHOICES AND TRADE-OFFS

The various SAR L2 processing choices explored in this report are summarized in Table 1.

Run reference	C2 L1B product	L2 SAR retracker model	Alpha_p LUT	Peel effect applied	Motivation
CNES	CPP	Numerical retracker	N/A	N/A	N/A
ESRIN R1	CPP	ESRIN SAM2	Yes	Yes	Full SAMOSA analytical model (Gaussian waves statistics)
NOC R2	CPP	NOC SAM3	No	No	Consistent with S3 DPM except for treatment of Thermal Noise. Only small dataset available for benchmarking.
ESRIN R3	CPP	ESRIN SAM3	Yes	Yes	To quantify impact on retrieval of omitting f1 term in SAMOSA3
ESRIN R4	CPP	ESRIN SAM3	Yes	No	Consistent with S3 DPM but with inclusion of alpha_p LUT
ESRIN R6	CPP	ESRIN SAM3	No	No	Consistent with S3 DPM baseline
ESRIN R5	ESRIN FBR	ESRIN SAM2	Yes	Yes	To explore impact at L2 of L1B processing choices

Table 1: Summary of SAR L2 experiments over ocean and coastal zone

Since the NOC R2 dataset includes only 10 individual tracks, this dataset is not included in the analyses.

3.1 R5 matching

Note the R5 dataset does not exactly match the CPP-based datasets, as the start/end time of the R5 FBR and the CPP products do not generally overlap. While it would be possible

to find the overlaps between R5 and CNES products, such a task is onerous and could not be performed in this study.

However, differences in sea state conditions sampled by each dataset could introduce uncertainty in the comparisons of the ESRIN FBR and CNES CPP results, particularly for the satellite/buoy collocations where the number of samples is small. Hence, dataset matching was performed at the level of the collocated satellite/buoy dataset to ensure that all runs (including R5 and CNES) correspond to exactly the same set of sea state conditions. This will be referred hereafter as “R5 matching”.

4 EXPERIMENTAL DATASETS

4.1 CNES Cryosat Prototype Products (CPP)

These are Cryosat-2 L1B SAR products generated by CNES in the context of the CP4O project and are referred to as the “CPP” products.

CPP data were generated and distributed by CNES to other partners in CP4O. The CPP dataset consisted of all Cryosat-2 data available in July 2012 and January 2013 in two regions: the Eastern North-Atlantic region (NAE) and the Central Pacific (PAC).

The validation in this report relates solely to the CPP data in the NAE region, where in situ data are available for independent validation, both in the open ocean and in the coastal zone.

Figure 1: Location of CPP Cryosat-2 L1B SAR products in the East North Atlantic region

4.2 Independent Data Sources

4.2.1 MOORED WAVE BUOYS

The wave buoy data used for validation consists of:

- Data from the UK Met Office and the WaveNet service, where buoys are generally located further than 25 km from land.
- Data from the UK Channel Coastal Observatory (CCO), where buoys are located within a few km of land.

The location of the buoys is shown in Figure 2 and Figure 3.

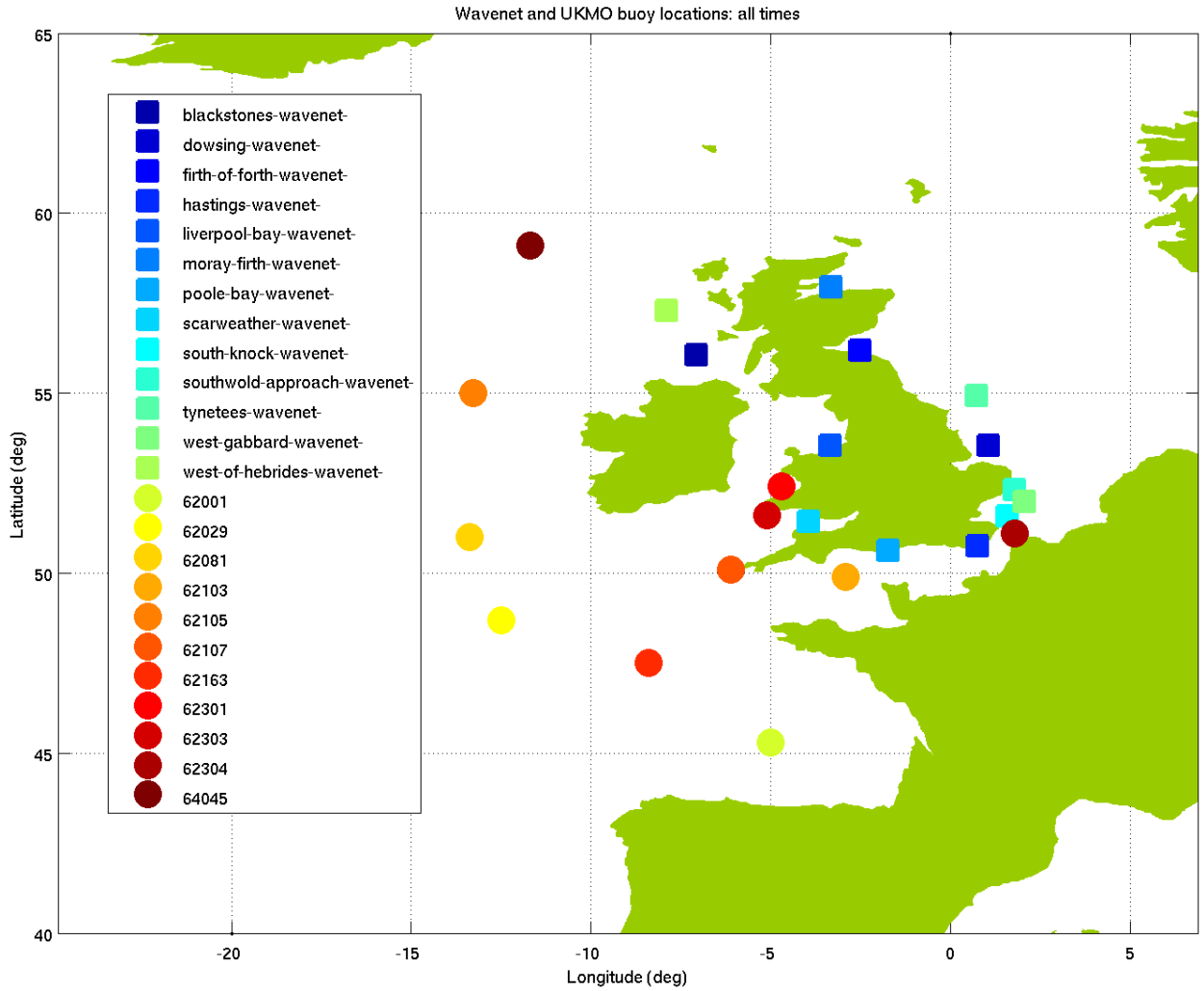

Figure 2: Location of UK Met Office and WaveNet wave buoys in the North Atlantic East region used for validation over the open ocean.

The analyses differentiate three cases:

- "Open ocean" buoy corresponding to a subset of UKMO buoys located far offshore (62001; 62029; 62081; 62105; 62163; 64045). This dataset is free of land contamination from nearby headlands, but is small and has the disadvantage that wave period (Tz) is reported only at 1 second resolution (as for all UKMO buoys)
- "Offshore" buoys corresponding to the full UKMO and WaveNet dataset. This dataset is larger but data are occasionally affected by land contamination. Wavenet buoys do however report wave period with a 0.1 second resolution.
- "Coastal" buoys corresponding to the CCO dataset. Located along the south coast of England, this dataset is selected specifically to assess the performance of C2 SAR in the coastal zone.

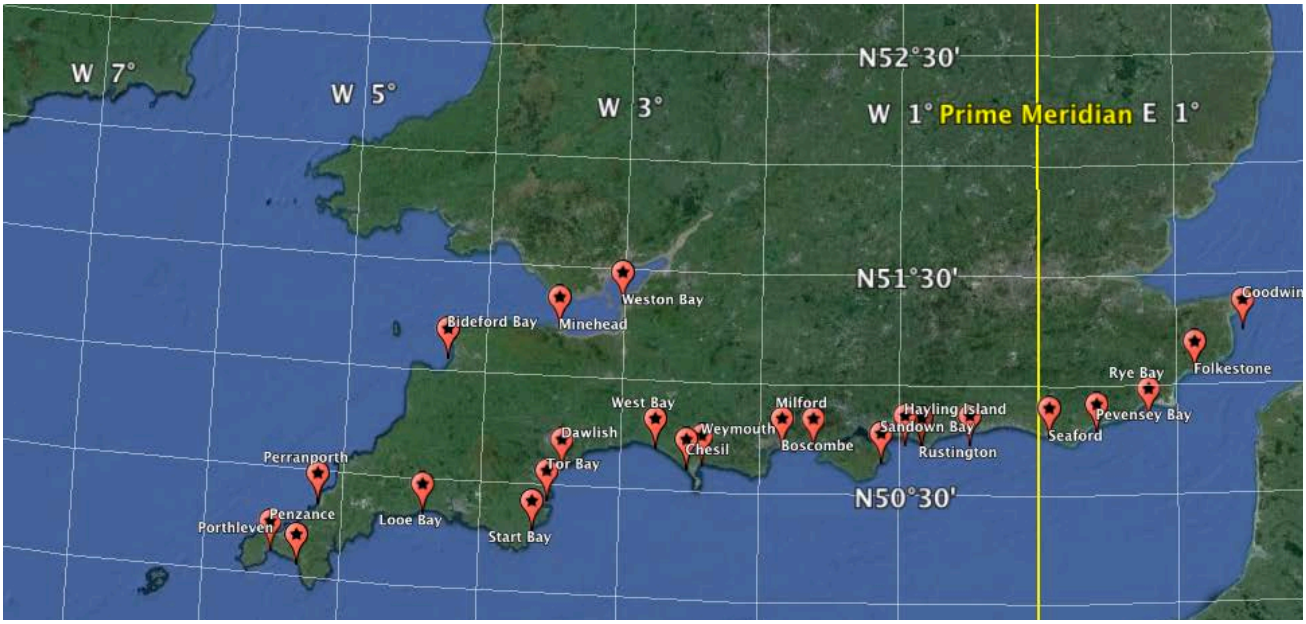

Figure 3: Location of Channel Coastal Observatory buoys in the North Atlantic East region used for validation over the coastal ocean.

4.2.2 SATELLITE ALTIMETERS

Other satellite altimeter data contemporary with the Cryosat products available in this study for validation consists solely of data from the Jason-2 mission. Unfortunately, no data were available for either Envisat or AltiKa in July 2012 and January 2013.

4.2.3 TIDE GAUGES

The Tide Gauge data are from the UK National Tide Gauge Network. The UK network includes 43 gauges (as shown in the maps in Section 7) most of which are related through the national levelling network to Ordnance Datum Newlyn. The whole network is owned by the Environment Agency and maintained by the Tide Gauge Inspectorate at National Oceanography Centre (NOC) under contract to the Environment Agency. Data are collected, processed and archived centrally to provide long time series of reliable and accurate sea levels, accessible via the British Oceanographic Data Centre at https://www.bodc.ac.uk/data/online_delivery/ntslf/

5 ALTIMETER DATA DIAGNOSTICS

The performance of the various SAR L2 processing choices are evaluated with the following diagnostics:

5.1 Misfit

This captures the quality of the fit between the L1B waveform and the fitted model, and is computed as:

misfit_CPP=100.*sqrt(1/104.*sum(residual^2)) Equation 1

with

residual=(model- data(13:116))./Max_data

Max_data=max(data(13:116))

data = waveform_data

model = waveform_model;

The misfit is particularly well suited to detect imperfect fitting, for example in the case of low SWH. Hence, together with the value of the misfit, its behaviour against SWH is also of interest.

Note that the misfit for the CNES CPP products was recomputed from the waveform data available in the CPP products using the expression in Equation 1.

5.2 Altimeter v Buoy SWH

Scatter plots of C2 SAR SWH versus buoy SWH are presented, supported by estimates of the mean and standard deviation of the SWH bias, where SWH bias is defined as:

$$SWH\_bias = SWH_{Alt} - SWH_{Buoy}$$

The dataset is obtained by collocating the altimeter data with the buoy, to within 1 hour and 50km. Careful data quality control needs to be applied to avoid altimeter data that may be contaminated by nearby land.

The same approach can be applied to other altimeter data e.g. Jason-2, thus supporting direct comparison of the performance of C2 SAR SWH with those of conventional LRM altimeters.

5.3 Distance to coast

Distance to coast was used to support the interpretation of the C2 SAR results, particularly in the coastal zone along the South coast of England. Figure 4 shows an illustration of the distance to coast obtained in the region of interest.

Distance to coast (d2c) was computed at a resolution of 0.01 deg (~ 1km) based on the high-resolution shorelines available via the NOAA Global Self-consistent, Hierarchical, High-resolution Geography Database (GSHHG;

http://www.ngdc.noaa.gov/mgg/shorelines/gshhs.html).

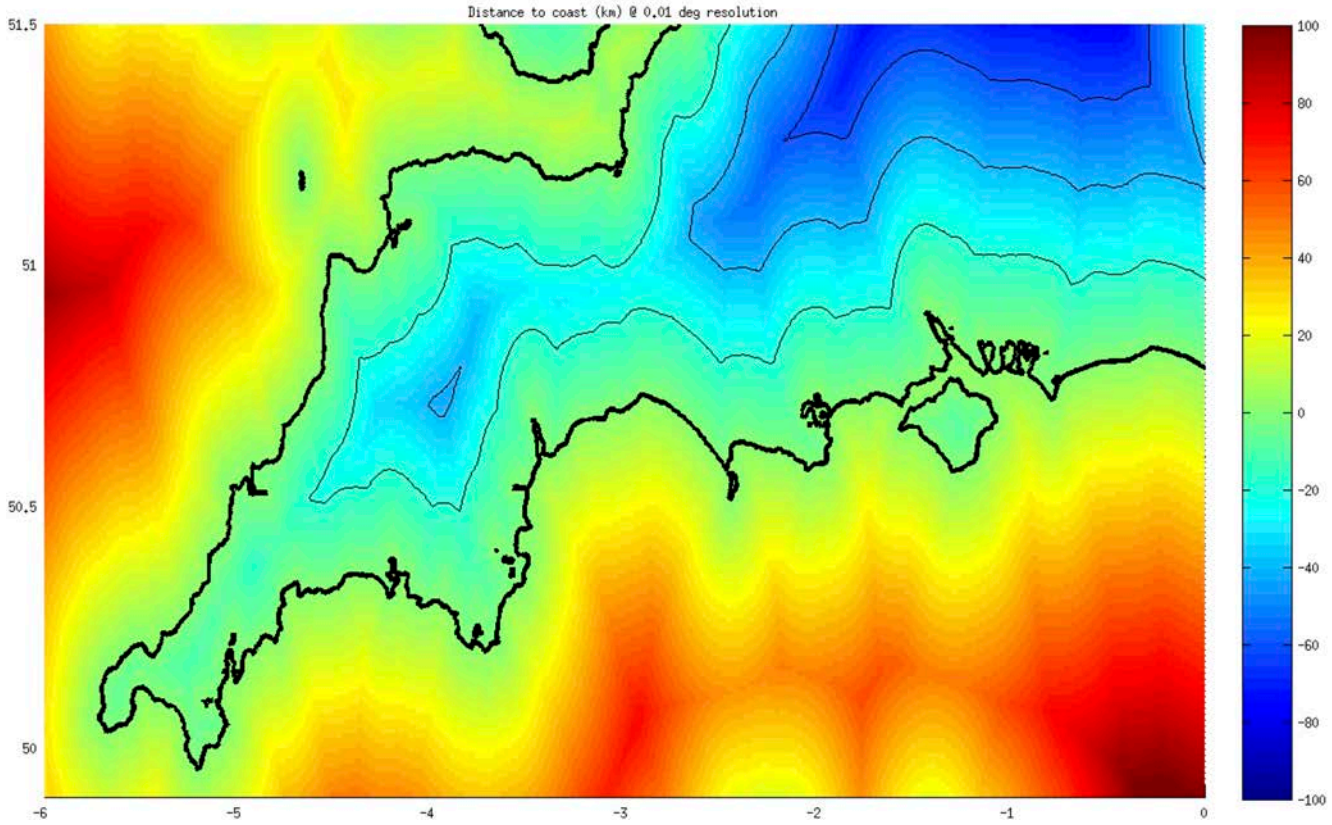

Figure 4: Distance to coast computed for the South West England coast at 0.01 deg resolution based on the NOAA GSHHG shoreline database.

6 OUTLIER REMOVAL

Various levels of outlier removal were applied to remove anomalous data and measurements contaminated by land echoes. The outlier removal procedures were applied in exactly the same way to the CNES and ESRIN data. Anomalous data in either datasets were removed from both, to ensure that the dataset remain exactly comparable.

7 RESULTS OVER THE OPEN OCEAN

In this section, we begin by presenting the results for the CNES and ESRIN R1 run. Key results for all runs are condensed in the form of tables in Section 0. For the sake of brevity, only some of the relevant plots for the other runs are provided in Appendix A.

7.1 CNES and ESRIN R1 results

7.1.1 TWO EXAMPLES

Figure 7 and Figure 7 show the CNES and ESRIN R1 results for two 300km data segments of C2 SAR L2 data near buoys located far offshore. The locations of the data segment and the buoy are shown in Figure 5.

The subplots show the 20Hz records of the following parameters (from top to bottom):

- Sea Surface height anomaly, computed for both CNES and ESRIN as the difference between the retrieved SSH (uncorrected for geophysical corrections) and Mean Sea Surface as provided in the ESRIN product.
- Significant Wave Height
- Pu
- Misfit.

The CNES and ESRIN R1 retracker show remarkable agreement for all fields, except Pu where a quasi-constant offset is observed.

In Example #1, conditions are stable over the 300km and both retrackers report misfit values around 2. Example #2 shows surface conditions that vary rapidly within a few km, even though the data is taken a long way from any land. The misfit is clearly able to detect these anomalous features. Accordingly, misfit can be used to detect outliers and here, data points with misfit values larger than 3 have been greyed out.

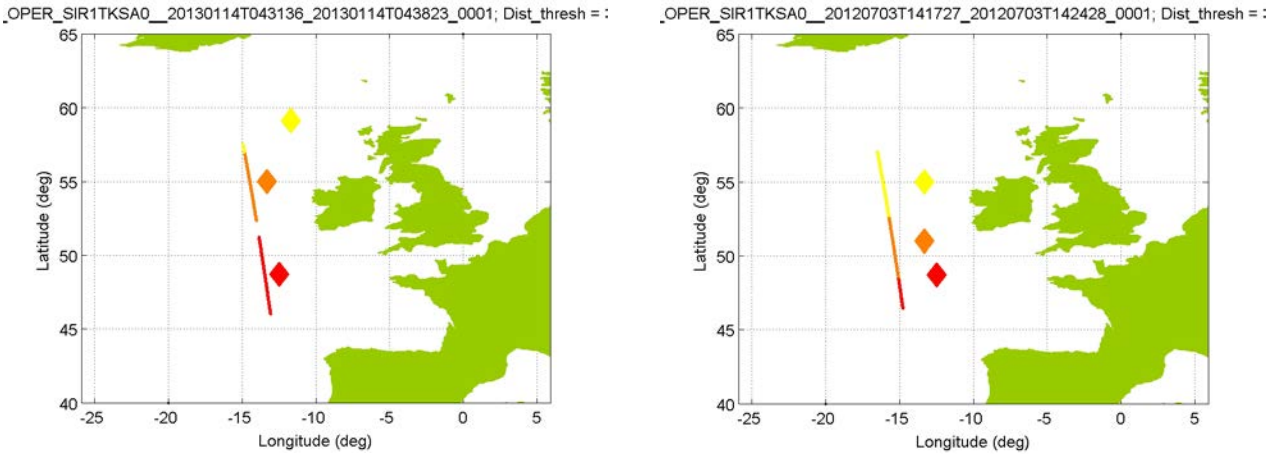

Figure 5: Location of C2 SAR data segment and collocated buoys for Example #1 and Example #2 shown in Figure 6 and Figure 7.

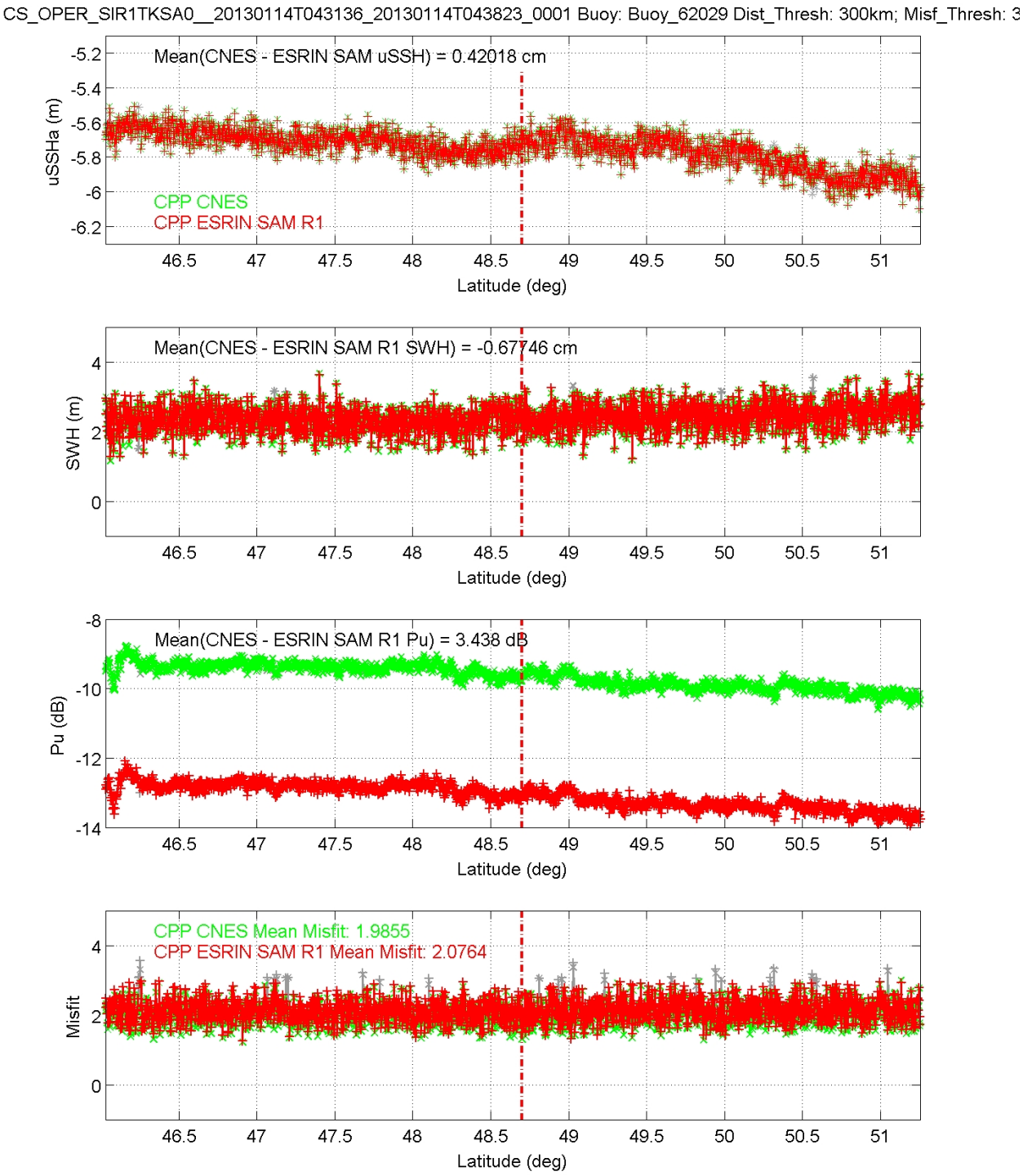

Figure 6: Example #1 of a 200km segment of C2 SAR data over buoy 62029 far offshore. The vertical dotted line represents the latitude of the buoy. The locations of the data segment and the buoy are shown in the inset map.

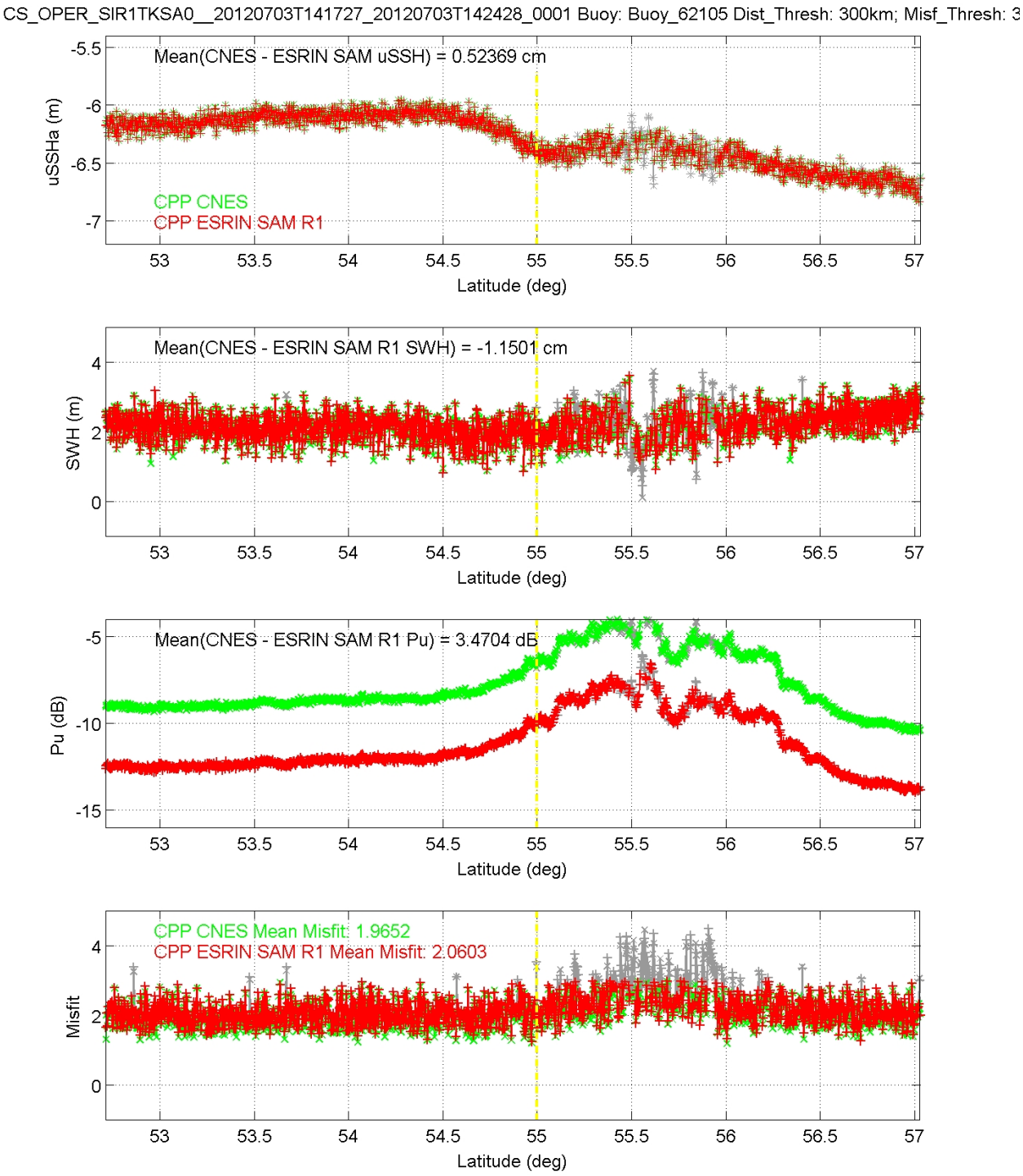

Figure 7: Example #2 of a 200km segment of C2 SAR data near UKMO buoy 62029. The vertical dotted line represents the latitude of the buoy. The location of the data segment is shown in the inset map.

Figure 9 and Figure 9 show the difference plots between the CNES and ESRIN R1 results for the data shown in Figure 6 and Figure 7 respectively. The figures also show the mean differences as legends in the plots. The mean difference for each parameter is calculated over the 50km closest to the buoy, which is indicated by the data highlighted in light blue.

In these examples, and in general, the agreement between CNES and ESRIN R1 results is extremely good, with average differences less than 0.5 cm for SSH and around 5 cm for SWH. The difference in Pu is also very stable across the data segment.

However, the difference plots reveal noticeable spikes in all parameters. These spikes are seen in most datasets. The spikes are not obvious in the data in Figure 7, so cannot be easily attributed to either retracker. There was no opportunity in this study to perform further analyses to determine the exact origin of these spikes.

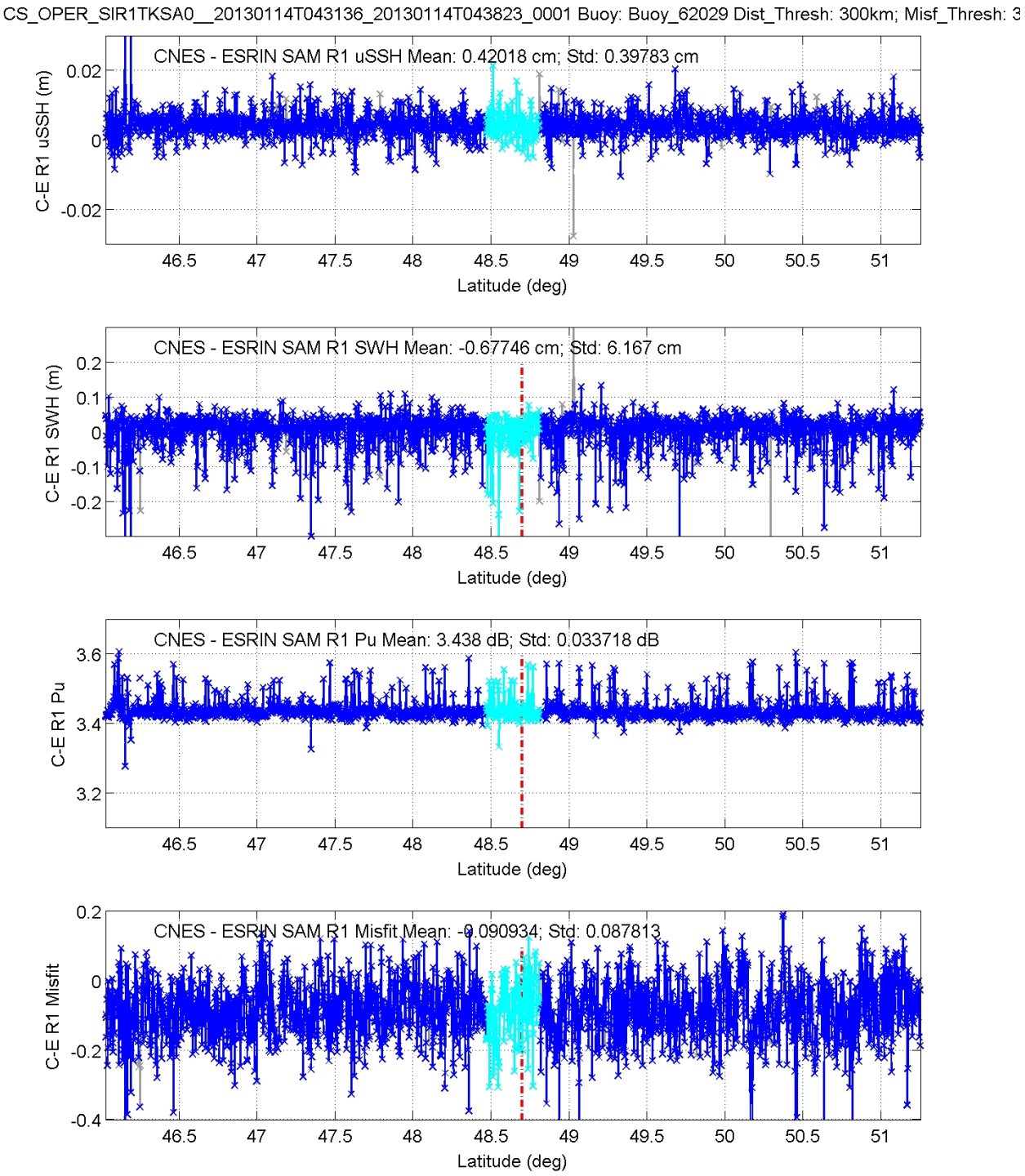

Figure 8: Difference plots between CNES and ESRIN R1 for the data in Figure 6.

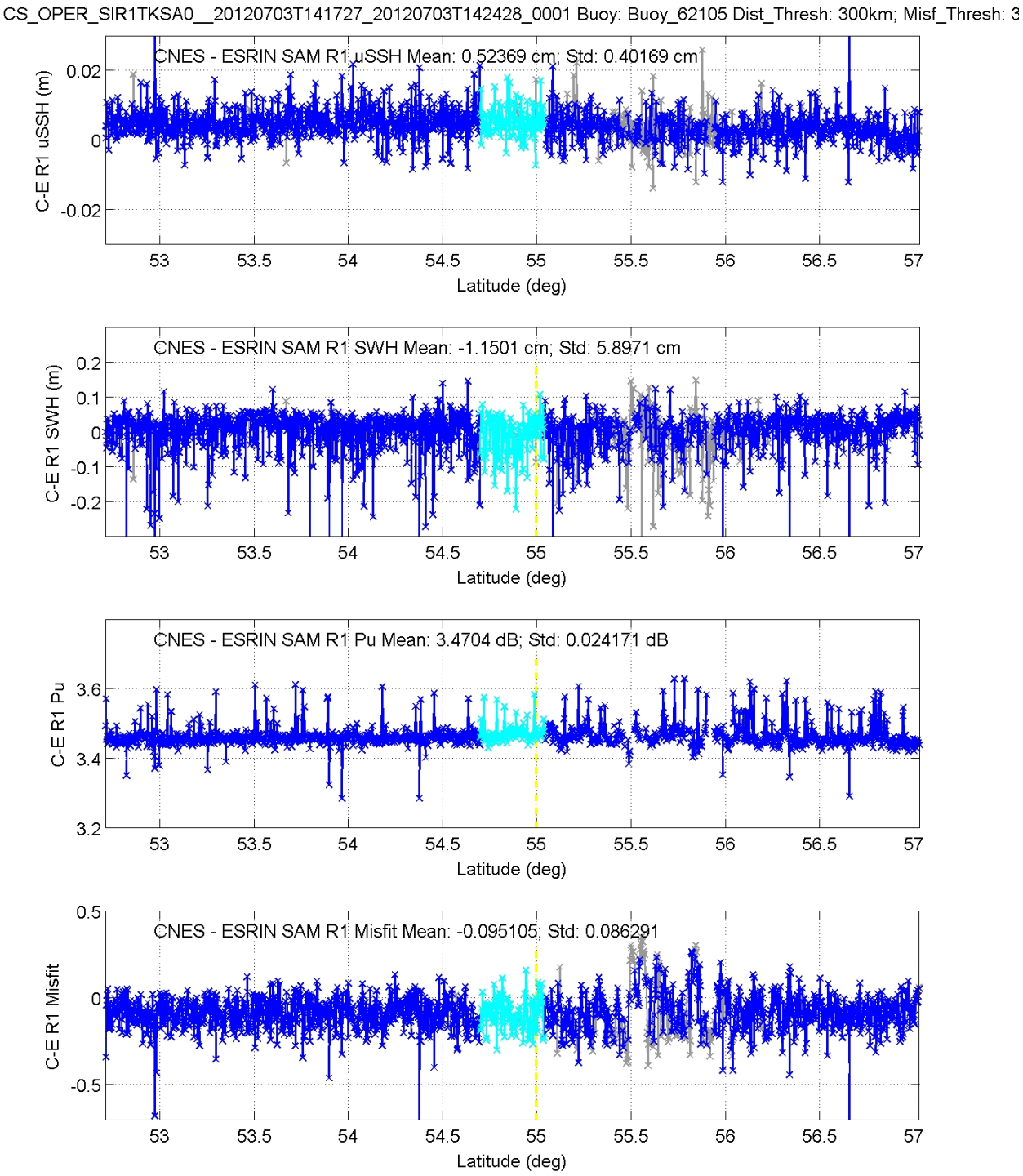

Figure 9: Difference plots between CNES and ESRIN R1 for the data in Figure 7.

7.1.2 OVERALL COMPARISONS

We now examine the overall performance of the retrackers by considering all data obtained within 50km of offshore buoys.

Figure 10 shows the distribution of the misfit against SWH for both the CNES (top) and the ESRIN R1 (bottom) results, with colour indicating the density of samples in a Log10 scale. These plots correspond to data obtained without any threshold applied to the misfit.

Note the stricking similarity between the two plots, both indicating that misfit increases with SWH. Some increase in misfit with SWH is expected, given the increase noise in measured waveforms in higher sea state.

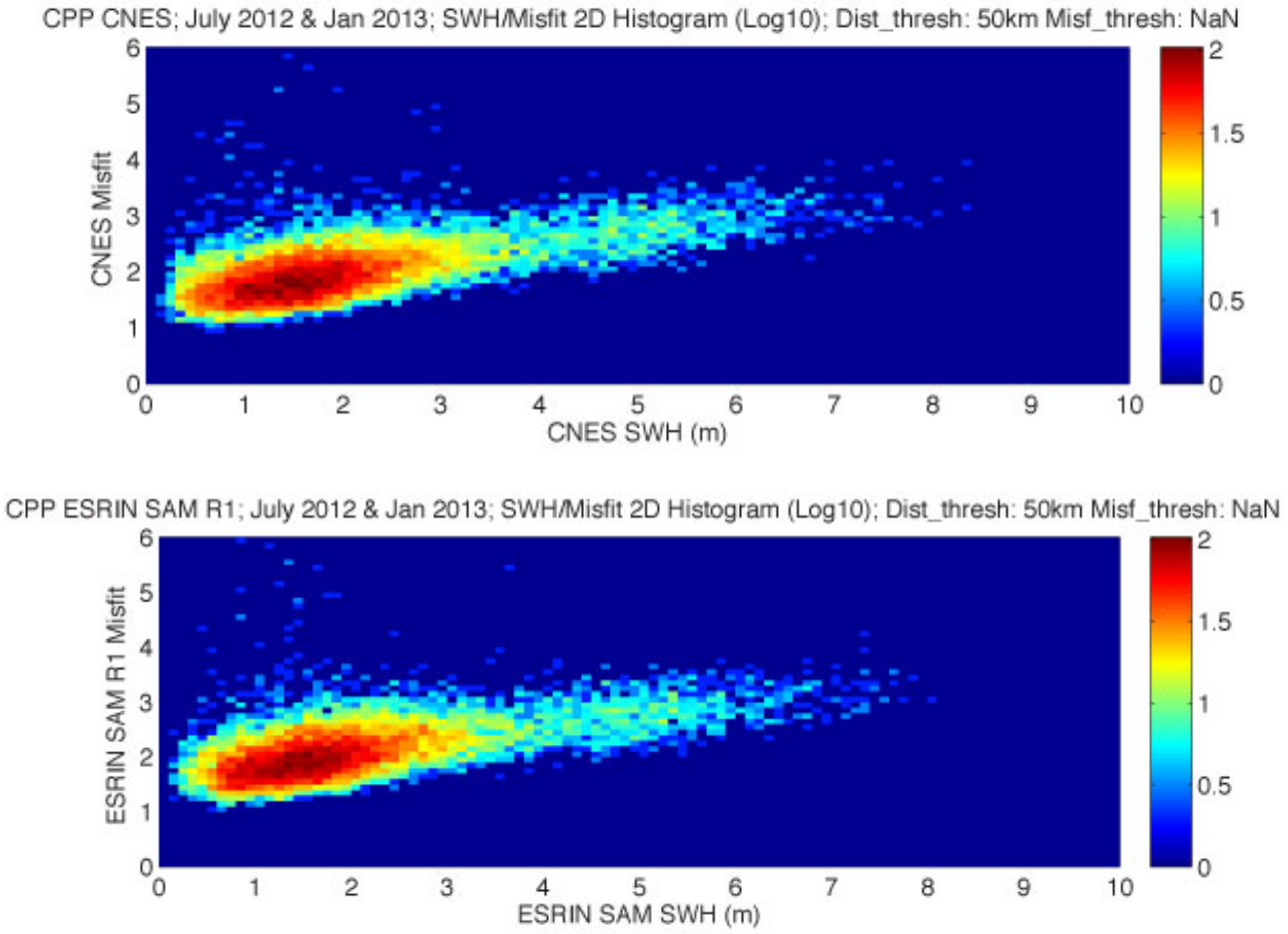

Figure 10: Misfit against SWH for (top) CNES and (bottom) ESRIN R1 results.

Figure 11 highlights the strong similarity between the misfit obtained with the ESRIN R1 and CNES retrackers over the full range. We note that the CNES misfit is, on average, slightly smaller.

Figure 12 shows the behaviour of the ESRIN R1 misfit against distance from coast, for all data obtained within 50km of all offshore buoys. Note the step-wise behaviour of the misfit within a few km of the coast. This indicates that:

- the "offshore" buoy dataset includes considerable data over land (mainly linked to the complex shape of the UK coastline), which will need to be flagged and removed.
- misfit further than 70km from land averages around 2, with a scatter of 0.33, suggesting that misfit values around 2 ± α * 0.33 (with α = 1,2 or 3) should generally correspond to good uncontaminated data.

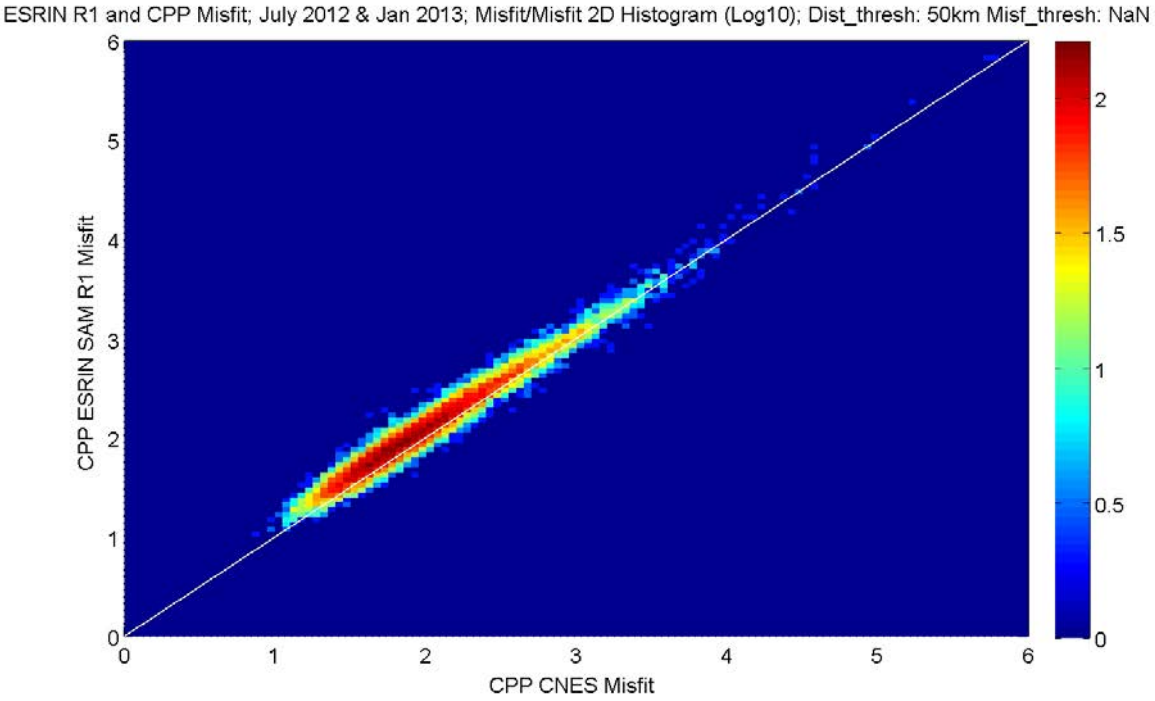

Figure 11: Scatter plot of ESRIN R1 misfit versus CNES misfit.

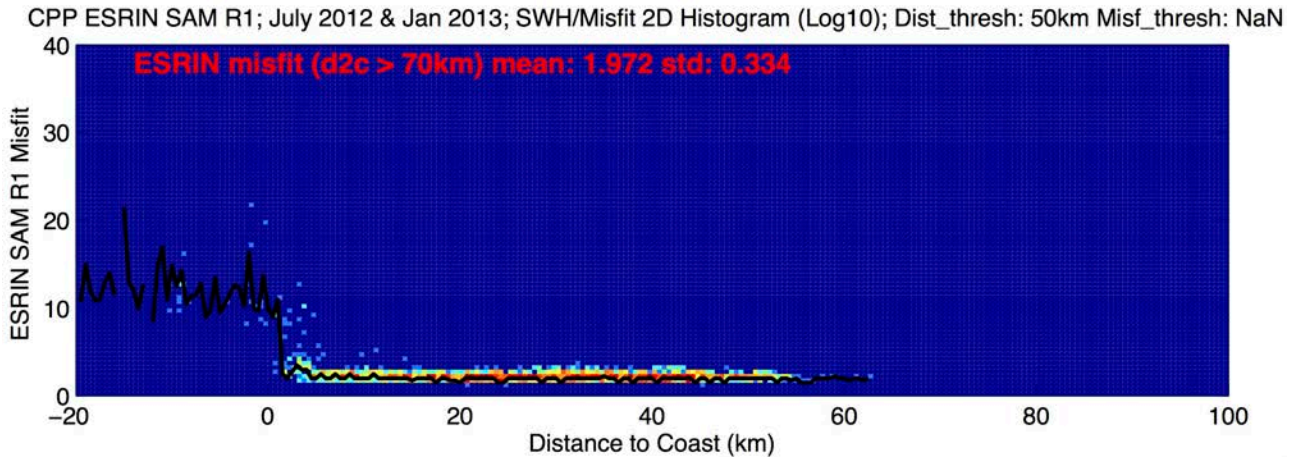

Figure 12: Misfit against distance to coast for the ESRIN R1 retracker, for all data within 50km from offshore buoys and no misfit threshold applied.

7.1.3 SCATTER PLOTS

Figure 13 shows the scatter plots of uncorrected SSH anomaly (uSSHa) for the ESRIN R1 and CNES retrackers for all offshore buoys (top) and open ocean buoys only (bottom). Figure 14 and Figure 15 show the equivalent results for SWH and Pu.

The agreement between ESRIN R1 and CNES is, again, excellent.

In all cases, a misfit threshold of 3 was applied, resulting in a much smaller dataset in the open ocean case, which explains in part the difference in the estimates of the mean biases between the two buoy datasets (see statistics in legends). Nevertheless, with the exception of the near-constant bias in Pu, the biases for uSSHa and SWH between the two retrackers are negligible, of the order of 1 millimeter or less for uSSHa and of 1cm for SWH.

Similar analyses were performed without the application of the misfit threshold (not shown). This was found to have detrimental effects on the results for the full offshore buoy dataset, but negligible effect on the open ocean dataset where the quality of the fit is generally very good.

7.1.4 TRENDS AGAINST SWH

Figure 16 presents the trends against SWH of the difference between the two retrackers for uSSHa, SWH and Pu. This is a useful way to detect differences between the retrackers in different SWH ranges. The trends are encapsulated by the coefficients of the linear fit shown in the legend, which are summarised for all runs in the tables in Section 0.

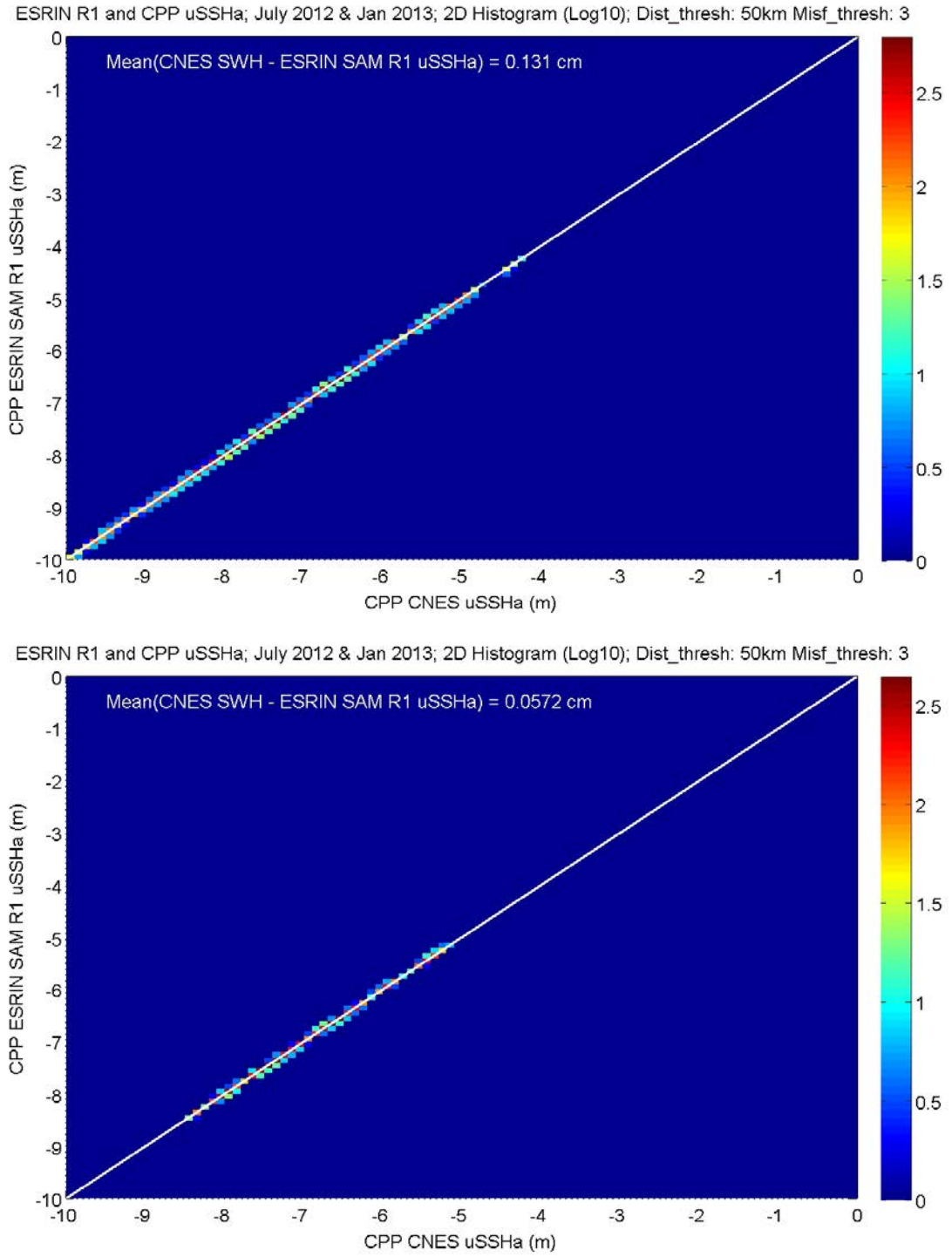

Figure 13: Scatter plot of uncorrected SSH anomaly (uSSHa) for ESRIN R1 versus CNES for (top) all offshore buoys (bottom) only open ocean buoys, with a misfit threshold of 3 applied.

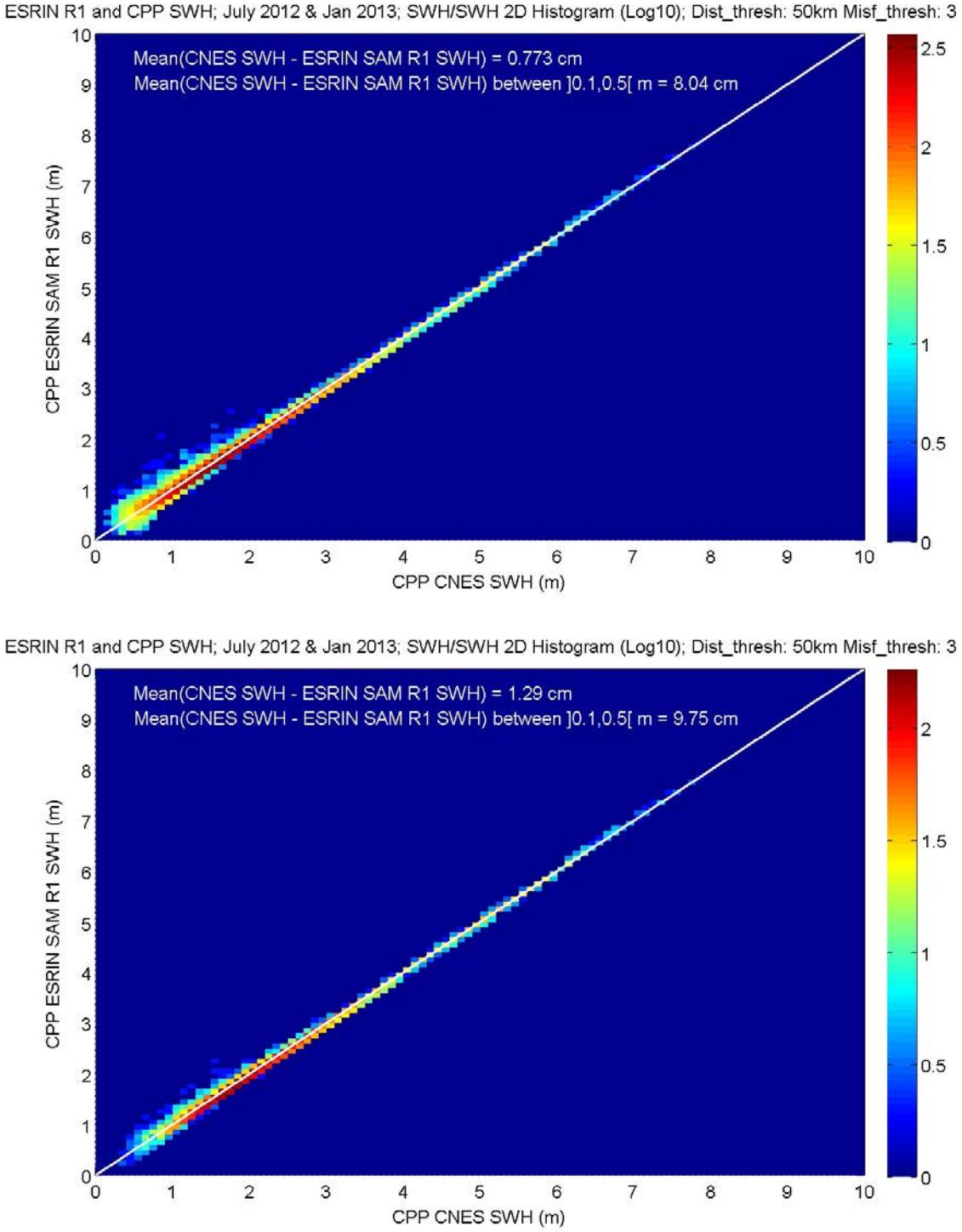

Figure 14: Scatter plot of SWH for ESRIN R1 versus CNES for (top) all offshore buoys (bottom) only open ocean buoys, with a misfit threshold of 3 applied. SWH values below 0.1 metres have been removed.

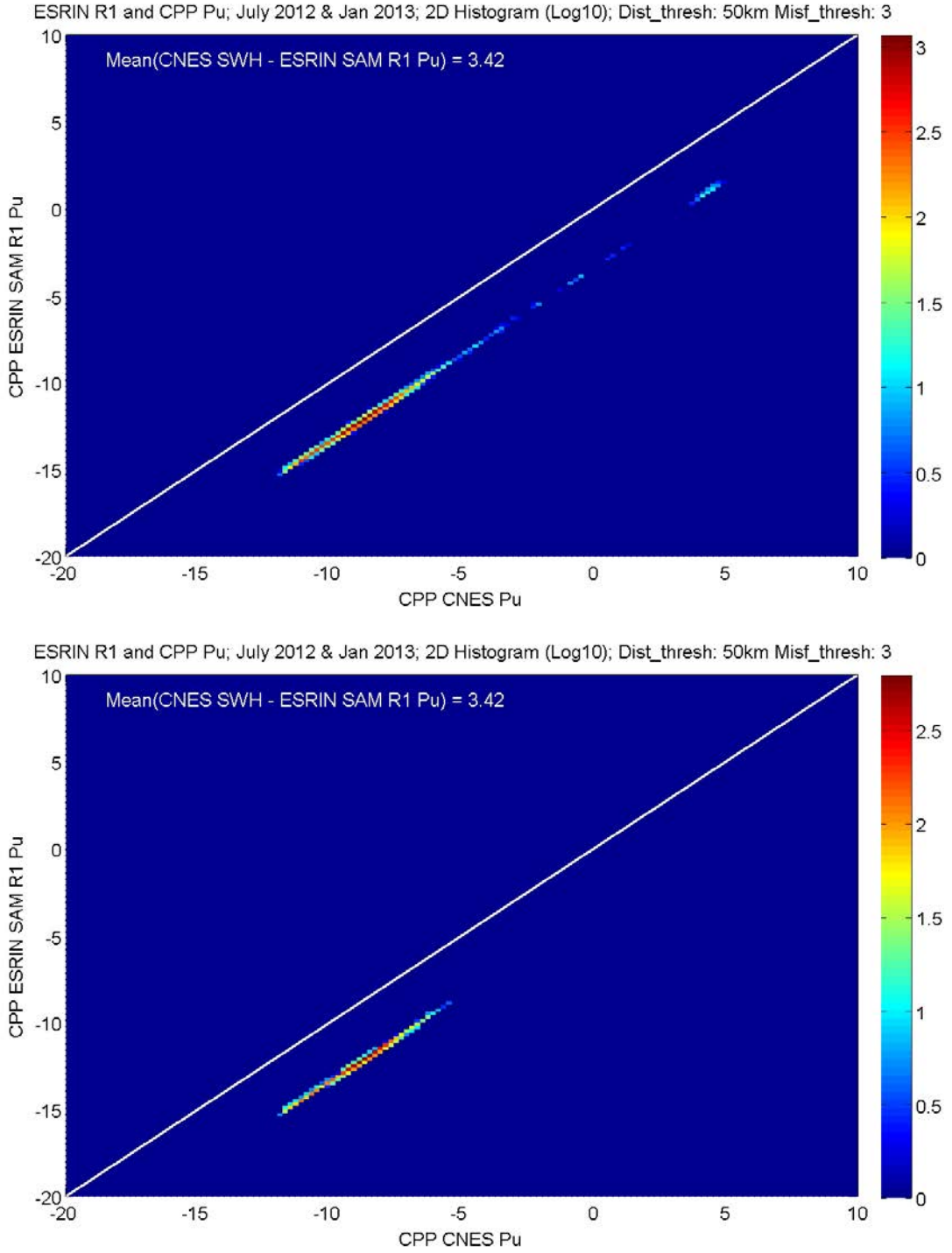

Figure 15: Scatter plot of Pu for ESRIN R1 versus CNES for (top) all offshore buoys (bottom) only open ocean buoys, with a misfit threshold of 3 applied.

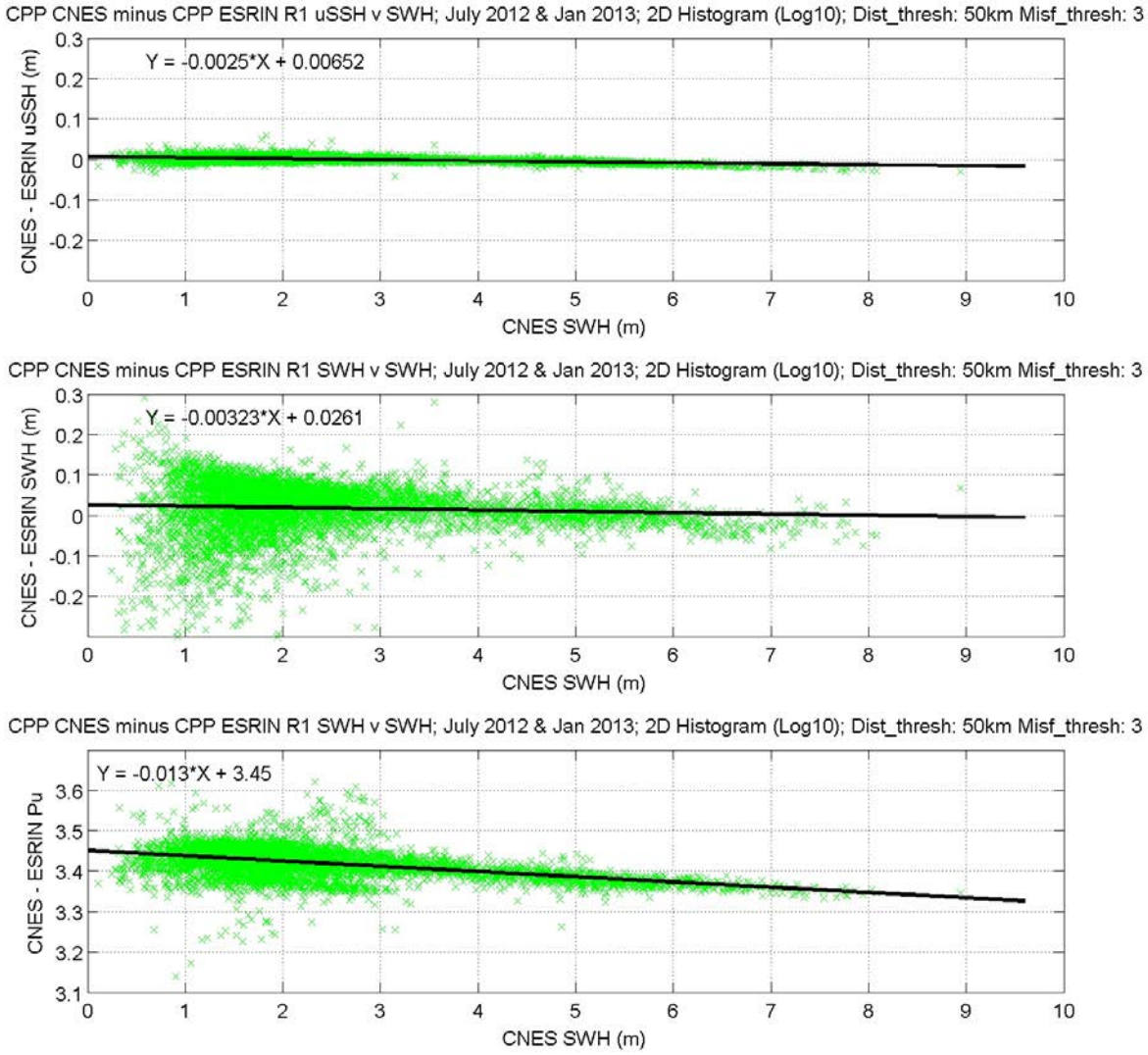

Figure 16: Behaviour and trend against CNES SWH of the CNES minus ESRIN R1 differences in (top) uSSHa (middle) SWH and (bottom) Pu, for the open ocean buoys only with a misfit threshold of 3 applied.

7.1.5 NOISE AS A FUNCTION OF SWH

7.1.5.1 METHODOLOGY

The noise (or variability) is estimated for SSH and SWH at 20Hz and presented as plots of Noise versus SWH. The noise is estimated as the standard deviation of all valid 20Hz measurements within 1 second, averaged over 6 seconds. This provides an estimate of the mean and the variability of the noise over approximately 50km. The variability is shown as error bars, provides a measure of the stability of the noise estimate, and helps with the detection of anomalous (non-uniform) conditions. Thus, additional outlier removal is applied to remove data where SSH or SWH display excessive variability, such as in the presence of oceanic or atmospheric features (unfortunately rather frequent in these data).

The noise at 1Hz is estimated by scaling by sqrt(20). The mean value of the 1Hz noise is reported at the standard value of SWH = 2 meters, corresponding to the average 1Hz noise observed for all datasets with SWH between 1.5m and 2.5m.

All statistics are computed for satellite data within 50km of each buoy. All datasets were "R5-matched" (see Section 3.1).

Analyses are made of the C2 data collocated with the full offshore buoys dataset and with the open-ocean buoys only. Various choices of misfit threshold were investigated. A misfit threshold of 2 results in complete loss of data. A misfit threshold of 3 results in only two valid estimates in the 2 meters Hs range, which is insufficient to provide reliable statistics. The cause of this large data loss in the computation of the noise is not entirely clear but could be linked to the spikes seen at 20Hz in Figure 8 and Figure 9. Recall that any anomalous value in either the CNES or ESRIN dataset is removed from both dataset, to maintain direct comparability.

Thus, analyses are presented for the results obtained for the open ocean buoys without the application of a misfit threshold (which is known to have a minor effect on open ocean results).

7.1.5.2 RESULTS

Figure 17 and Figure 18 present the 20Hz noise in SSH and SWH respectively, as a function of significant wave height, Hs, measured by the buoy collocated with the satellite. In each case, the bottom subplot also shows the noise estimates from the Jason-2 LRM data obtained for the same set of buoys over the same two months.

For SSH (

Figure 17), the results are consistent with previous findings i.e. SAR SSH 1Hz noise for Hs = 2 meters is around 1.2 cm while it is around 1.5 cm for Jason-2 LRM. There is a small difference between the CNES and ESRIN R1 results, CNES reporting a value of 1.254 cm compared to 1.223 cm for ESRIN R1. Although the differences and the dataset are small, the difference between the two retrackers could be considered significant, since outlier removal and collocated buoy samples are an exact match for both retrackers.

For SWH (Figure 18), the results are again consistent with previous findings. SWH 1Hz noise for Hs = 2 meters is around 8.6 cm for CPP SAR compared to 11.1 cm for Jason-2

LRM. Here again, there is a small difference between the CNES (8.74cm) and ESRIN R1 (8.62 cm) results.

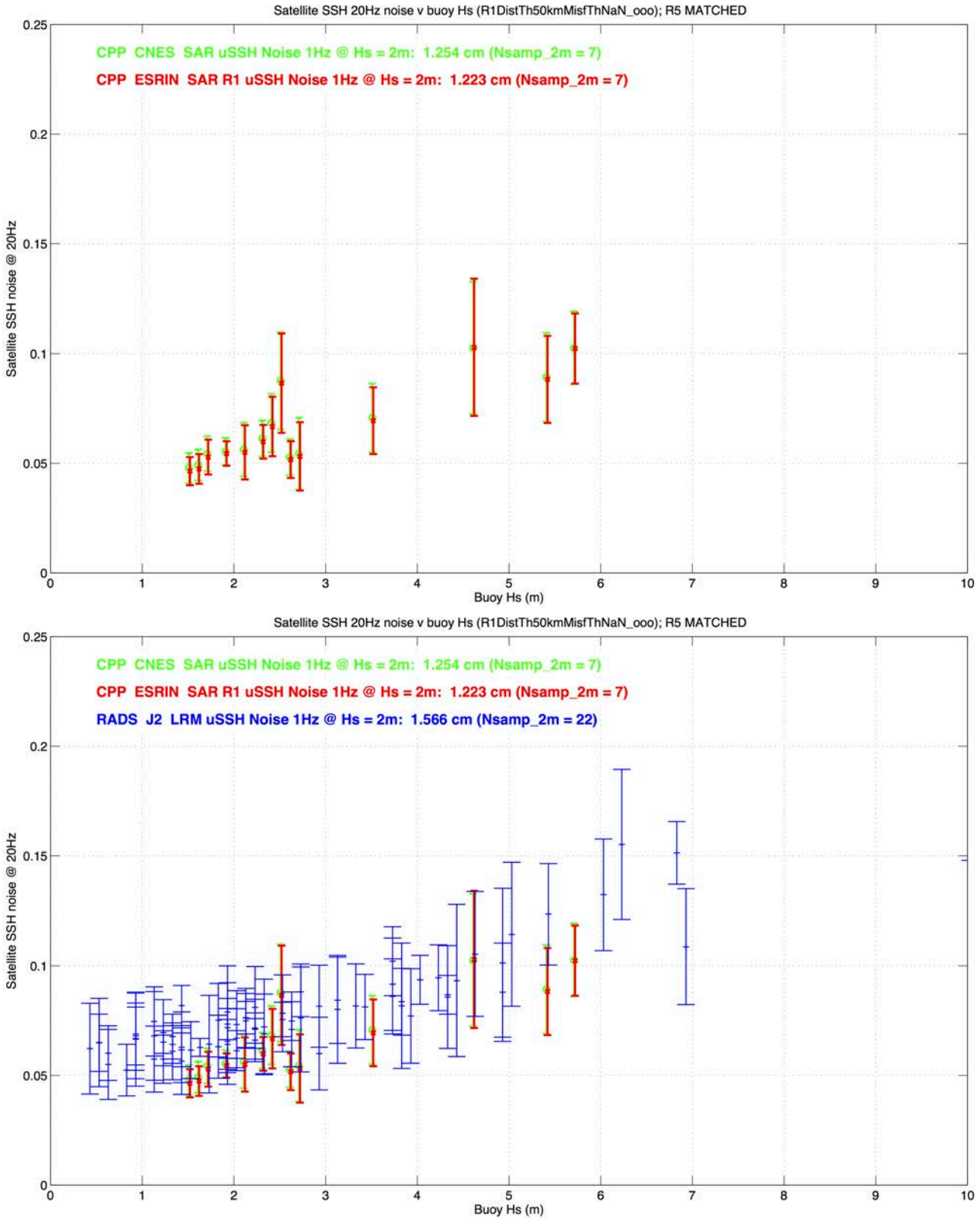

Figure 17: SSH 20Hz Noise against buoy Hs for (top) CNES and ESRIN R1 C2 SAR (bottom) same with Jason-2 LRM at the same (open ocean) buoys over the same period.

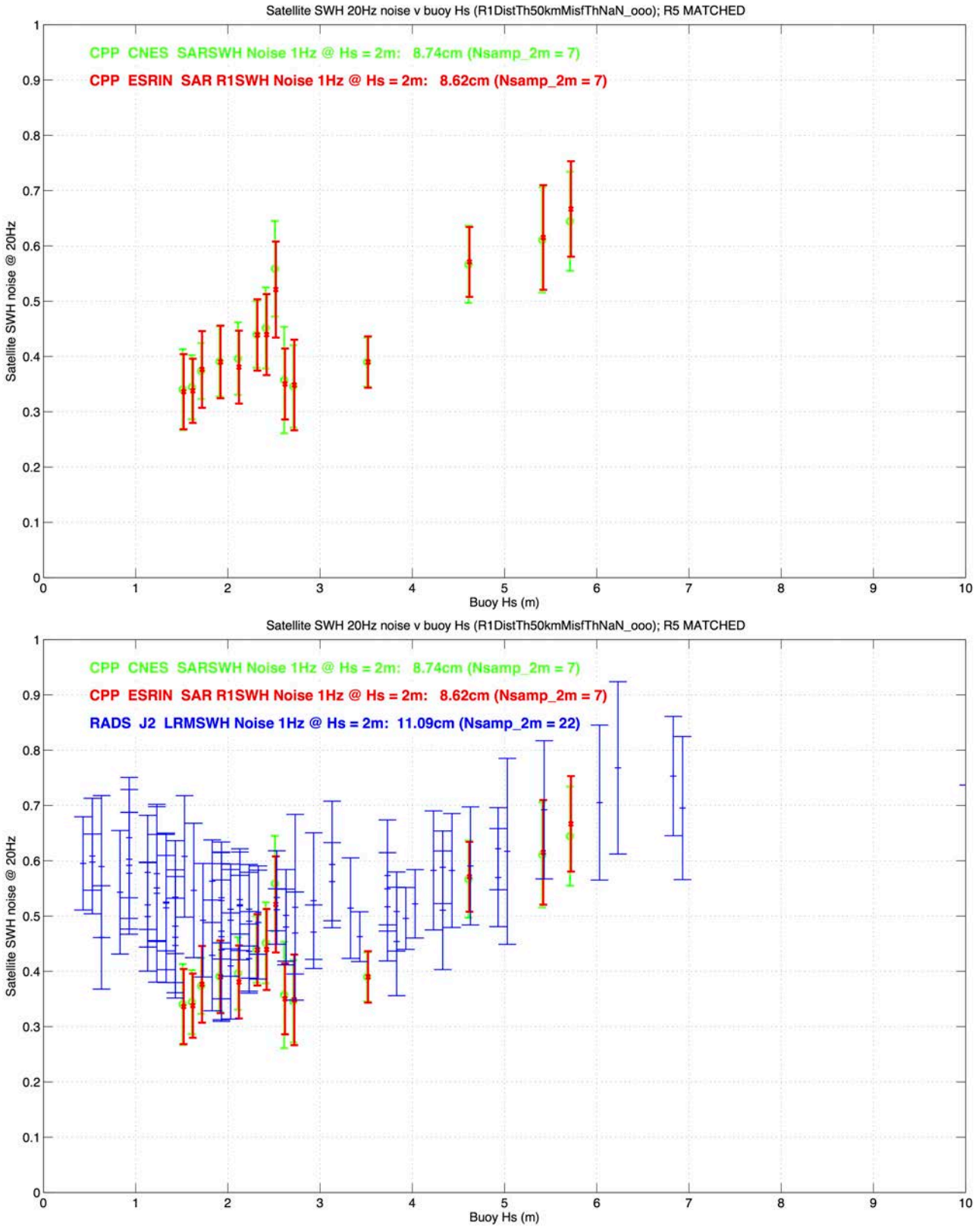

Figure 18: SWH 20Hz Noise against buoy Hs for (top) CNES and ESRIN R1 C2 SAR (bottom) same with Jason-2 LRM at the same (open ocean) buoys over the same period.

7.1.6 SSH NOISE AND SWH NOISE AS A FUNCTION OF TZ

The next set of figures present the 20Hz noise in SSH and SWH as a function of buoy Tz. (see Figure 19 and Figure 20). Here, the main interest is to observe the evolution of the noise with increasing wave period, rather than to obtain precise estimates of the noise in specific conditions.

Unfortunately, the open ocean dataset consists of data only from UKMO buoys, which report wave period at a fairly coarse 1 second resolution. Nevertheless, the dataset happens to span a good range of wave period, making it possible to make some observations about the behaviour with wave period. We find that:

- Both retrackers show similar response with wave period.
- For both SSH and SWH, the 20Hz noise increases with wave period i.e. in the presence of longer waves.
- There is some indication that the same also holds true for Jason-2 LRM data.

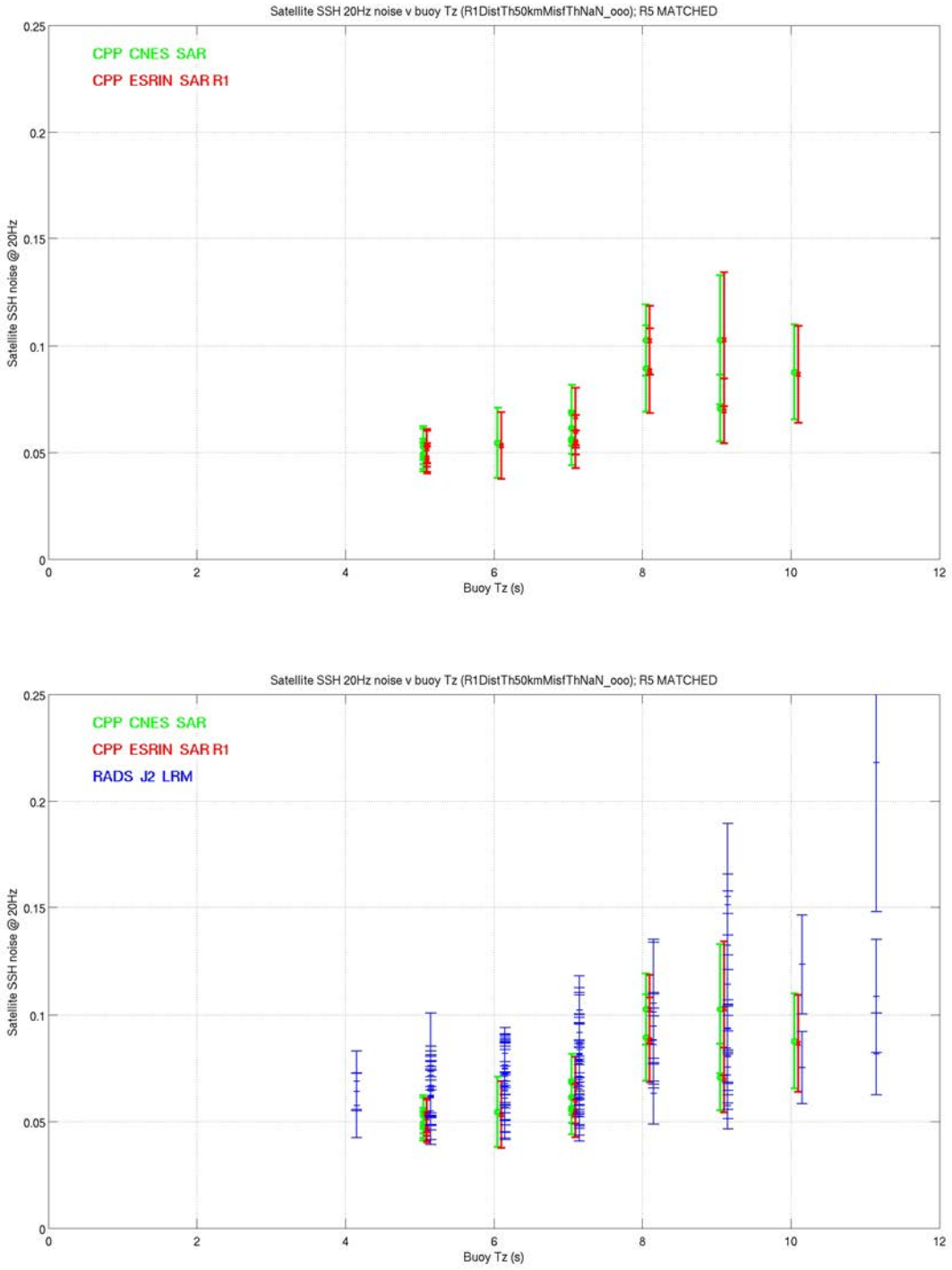

Figure 19: SSH 20Hz Noise against buoy Tz for (top) CNES and ESRIN R1 C2 SAR and (bottom) same Jason-2 LRM at the same buoy over the same period. Data corresponds to open ocean buoys only.

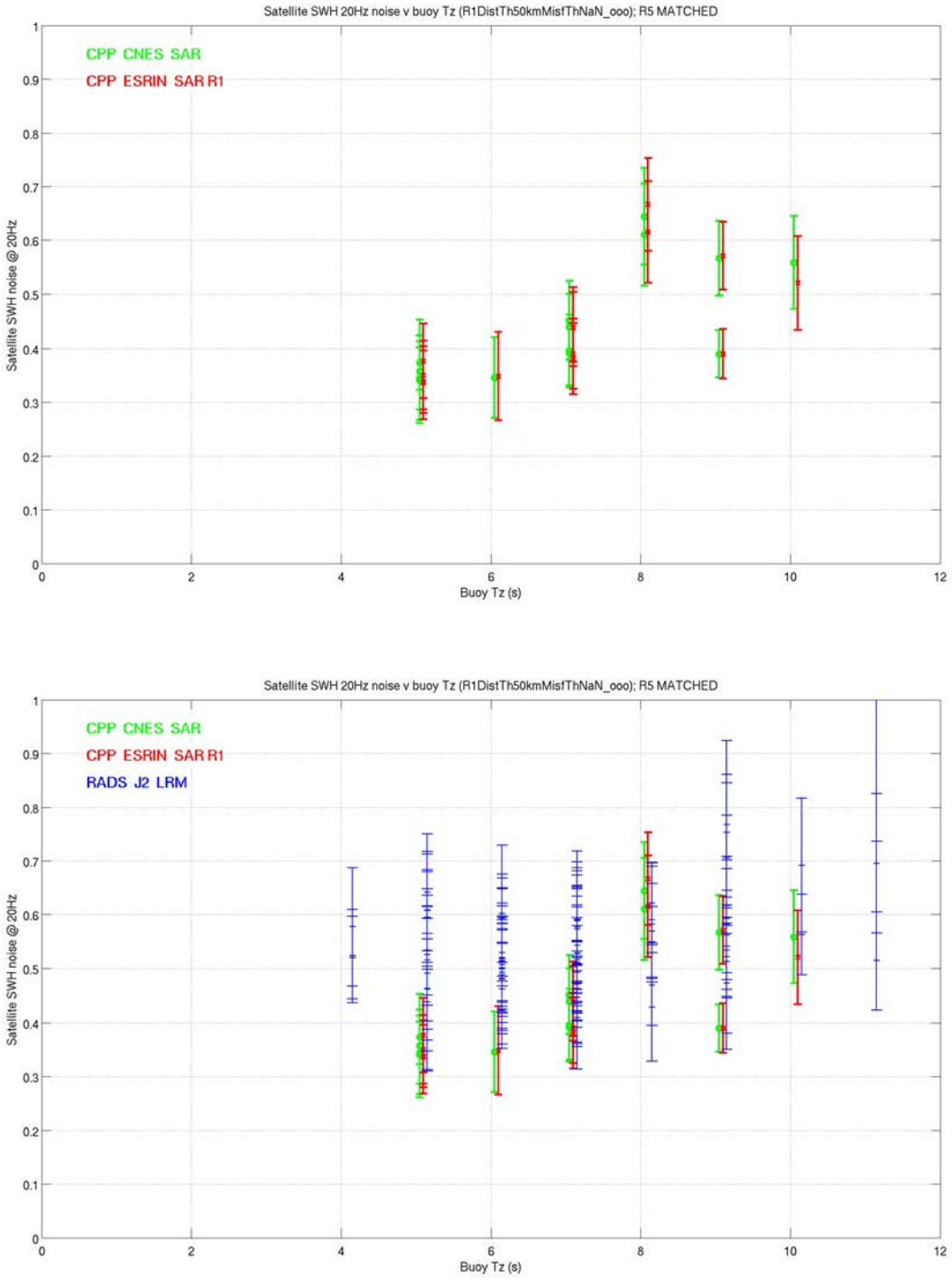

Figure 20: Same as for Figure 19 but for SWH 20Hz Noise.

7.1.7 SATELLITE SWH VERSUS BUOY HS

The validation of C2 SAR SWH against buoy Hs was performed for various collocated buoy datasets and choices of misfit threshold. Once again, the application of a misfit threshold leads to much smaller datasets, which sometimes prevent meaningful statistical estimation.

We first present in Figure 21 the results obtained by collocating C2 SAR within 50km of all offshore buoys after the application of a misfit threshold of 3. Applying a threshold value of 2 results in a complete loss of data.

We note that the number of samples is reasonably large (53) and that the CNES and ESRIN R1 retrackers give similar results in all cases. However, both CNES and ESRIN R1 display a significant bias against the buoys of around 20 cm. Hence, a misfit threshold of 3 is not sufficient to prevent a significant bias in C2 SAR SWH.

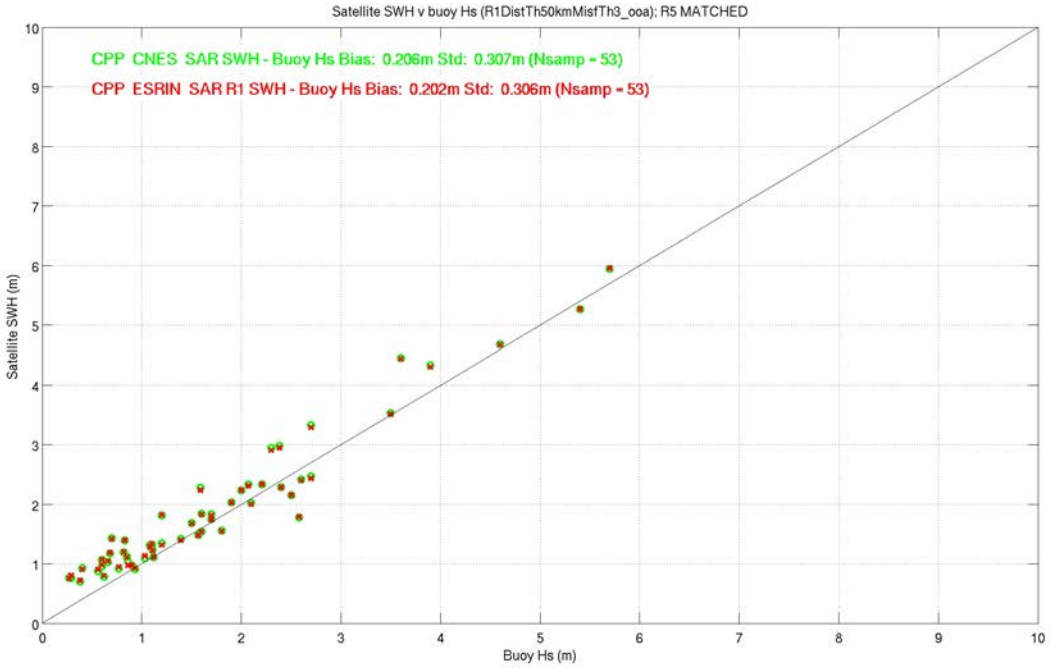

Figure 21: C2 SAR SWH from CNES and ESRIN R1 against buoy Hs for all offshore buoys and a misfit threshold of 3.

Figure 22 shows the same analysis but for the open ocean buoys only, and without the application of a misfit threshold. The number of samples is much reduced (19) but the bias against buoy Hs is now significantly smaller, down to 5 cm.

Figure 23 shows the same analysis, again for the open buoys only, but this time with a misfit threshold of 3 applied. The number of samples remains the same (19) but the bias decreases further, for both CNES and ESRIN R1, now reaching below 4 cm.

For comparison, Figure 24 shows the equivalent results for Jason-2 LRM, which reports a small bias below 8 cm. In all cases, the scatter is of the order of 22 cm.

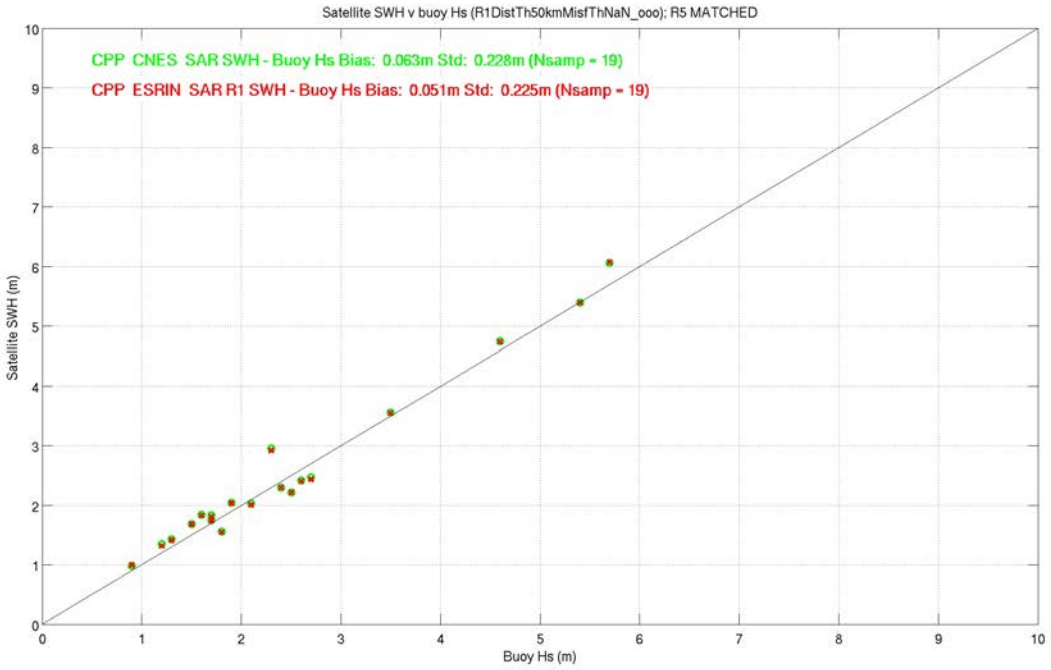

Figure 22: Same as Figure 21 for open ocean buoys only and no misfit threshold applied.

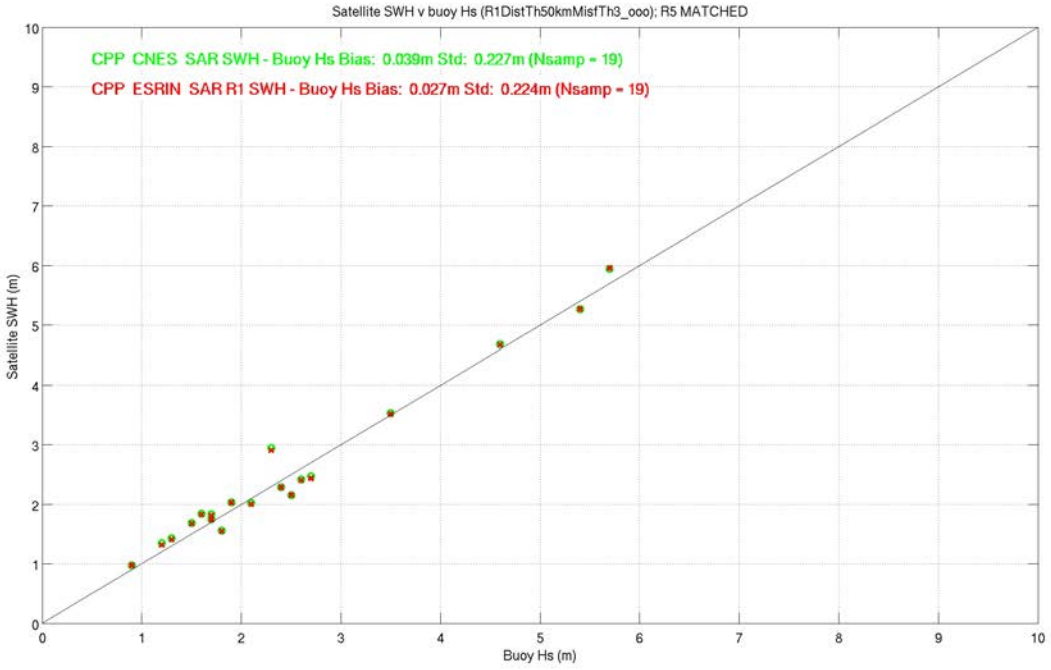

Figure 23: Same as Figure 22 for open ocean buoys only and a misfit threshold of 3.

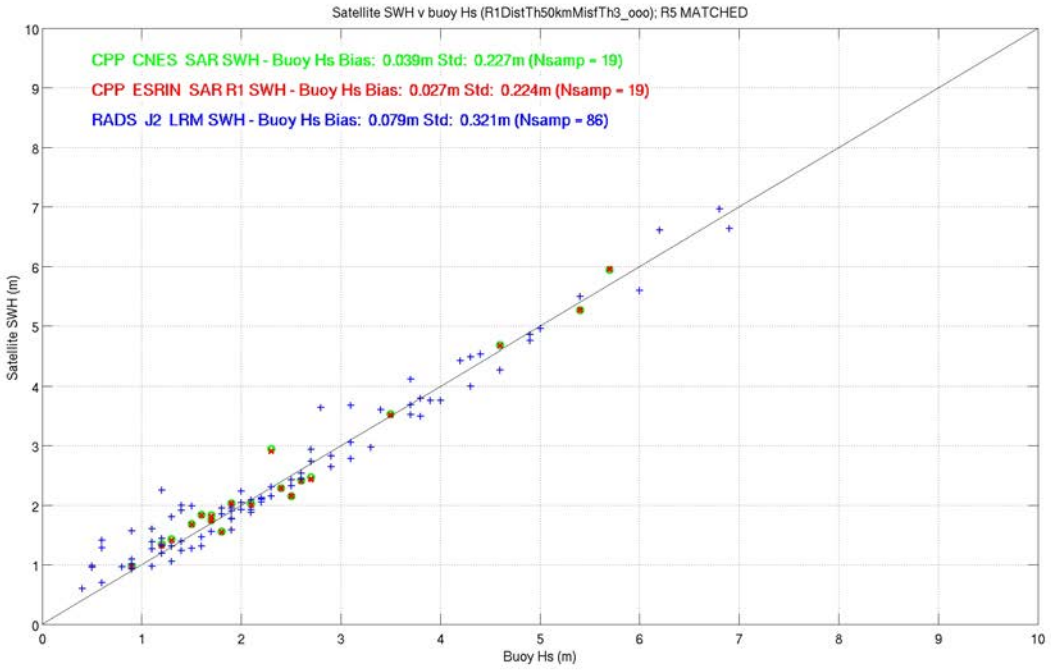

Figure 24: Same as Figure 23 with the inclusion of results for Jason-2 LRM.

7.2 ESRIN R5 results

We present here briefly the results for the ESRIN R5 data, which are based on L1B waveforms derived from the Cryosat-2 FBR with ESRIN in-house processing.

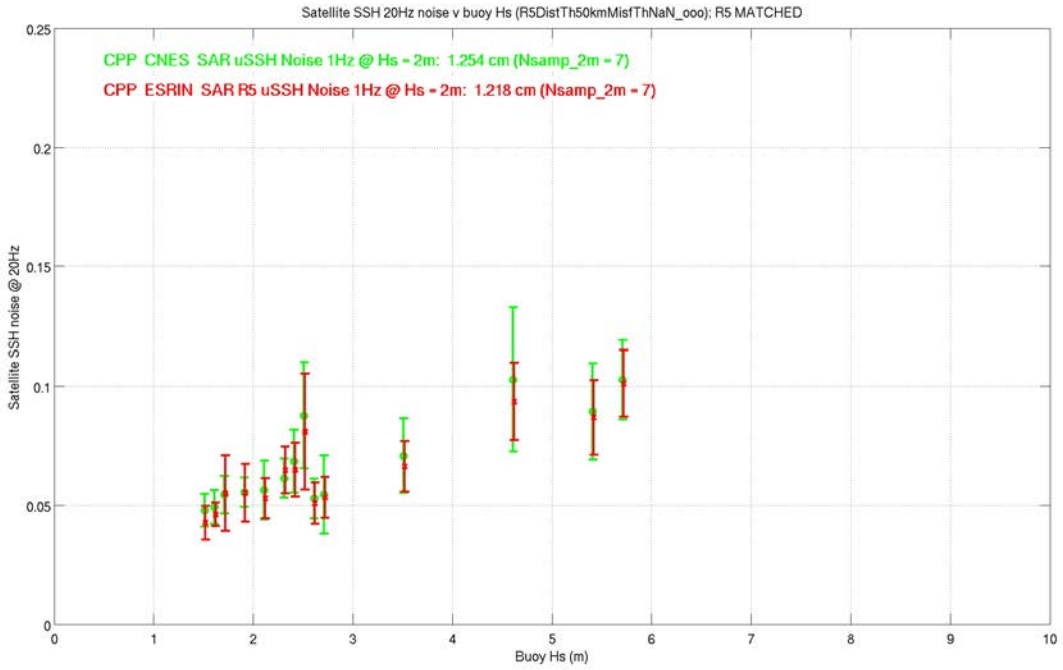

Figure 25: C2 SAR SSH 20Hz Noise against buoy Hs for CNES and ESRIN R5.

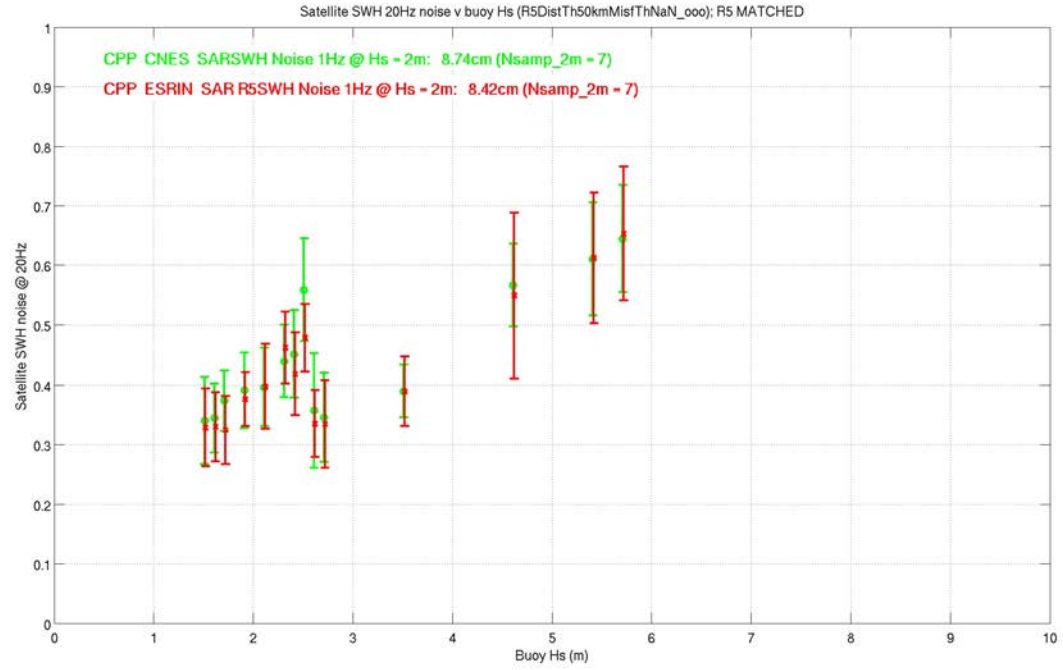

Figure 26: C2 SAR SWH 20Hz Noise against buoy Hs for CNES and ESRIN R5.

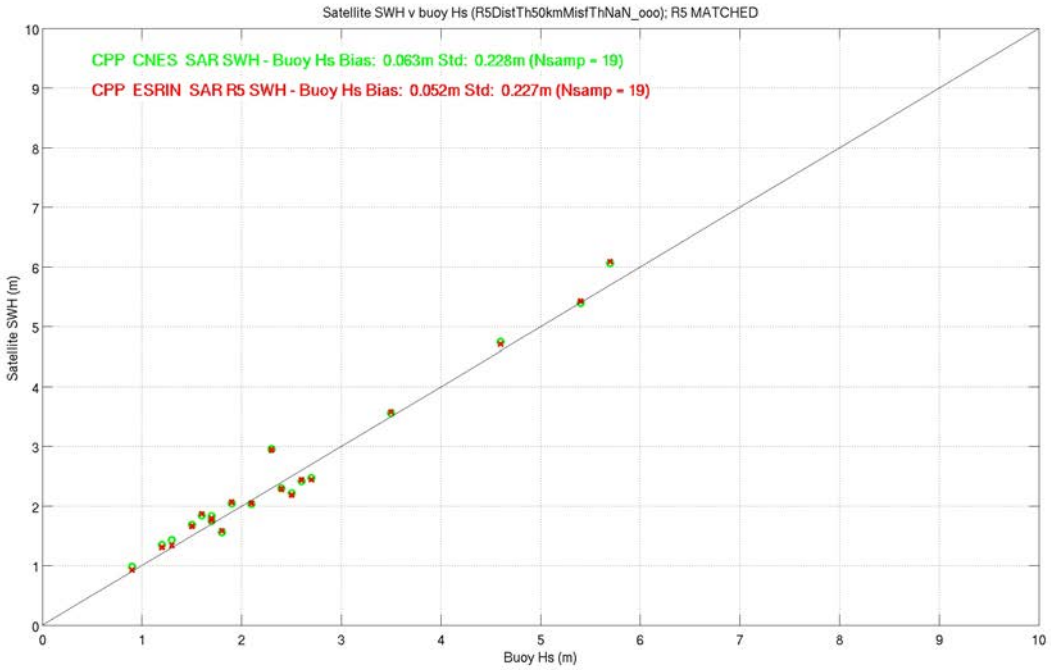

Figure 27: C2 SAR SWH from CNES and ESRIN R5 against buoy Hs for open ocean buoys only and no misfit threshold applied.

7.3 Result summary and conclusions for Open Ocean

The results for all runs are summarised in Table 2.

The main findings from these analyses are:

- There is excellent agreement between the results of various SAMOSA SAR retrackers and the CNES numerical retracker. ESRIN R1, R3 and R5 perform particularly strongly, occasionally exceeding the performance of the CNES SAR numerical retracker in terms of noise and (marginally) validation of SWH against buoy Hs.
- ESRIN R4 and R6 show the most marked difference from the CNES results.
- By focussing on open ocean buoys only and adopting very careful data editing, C2 SAR SWH shows no bias against buoys in the open ocean. However, even small increases in misfit will result in unacceptable biases in SWH.
- New results for SAR SSH and SWH noise as a function of Hs confirm previous findings about the performance of SAR altimetry with regards to reduced noise in comparison with LRM.

The activities raised the following issues which will need further investigation:

- Analyses were hampered by the small size of the datasets, which made results especially sensitive to the precise make-up of the datasets and to the details of the outlier removal procedure. Analyses of larger datasets are required in order to obtain more robust statistical results and estimates of the uncertainty.
- The use of misfit for data editing should be further explored.
- Further analysis is required of the origin of the spikes observed in the difference plots between the ESRIN and CNES results (e.g. Figure 8). It is thought that these spikes could be responsible for the large data loss observed when computing noise statistics. New and more robust methods to evaluate noise statistics could also be beneficial.

Table 2: Summary diagnostics for C2 SAR CNES and ESRIN L2 results

Run reference	1Hz Noise @ 2m		SWH v buoy Hs		CNES – ESRIN difference			CNES – ESRIN against SWH (trend)		
	SSH (cm)	SWH (cm)	Bias (cm)	Std (cm)	SSH (cm)	SWH (cm)	Pu	SSH (cm/m)	SWH (cm/m)	Pu (units/m)
CNES	1.254	8.74	6.3	22.8	-	-	-	-	-	-
ESRIN R1	1.223	8.62	5.1	22.5	-0.0	1.2	3.42	-0.28	0.39	-0.013
ESRIN R3	1.246	8.58	5.0	22.5	1.7	1.2	-14.1	1.05	-0.22	-0.011
ESRIN R4	1.246	8.52	-15.8	22.2	-0.3	22.4	-13.9	0.11	2.81	-0.001
ESRIN R6	1.250	9.25	-10.9	25.4	-0.3	17.4	-13.9	0.11	-4.76	0.002
ESRIN R5	1.218	8.42	5.2	22.7	N/A	N/A	N/A	N/A	N/A	N/A
Jason-2	1.566	11.09	7.9	32.1	N/A	N/A	N/A	N/A	N/A	N/A
Notes	Open-ocean No misfit threshold		Open-ocean No misfit threshold		Open-ocean No misfit threshold			Open-ocean No misfit threshold		

8 RESULTS IN THE COASTAL ZONE

This section details the validation study carried out for ESRIN R1 C2 SAR data around the coasts of the UK using tide gauges. Tide Gauge data was obtained from the UK Tide Gauge Network available from BODC and described in section 4.2.3.

Validation was carried out also for all CNES and ESRIN runs against coastal wave buoys from the Channel Coastal Observatory (see section 4.2.1). However, those results are not presented here as there was no time to perform in-depth analyses and reporting.

8.1 Validation strategy and results

For satellite missions with a repeat orbit pattern, validation can be naturally carried out by comparing time series of heights in each point along track of the altimeter with the time series of the sea level measured by the tide gauges at the times of each satellite overpass, as done for instance in [RD5]. This is not possible for Cryosat-2 due to the very long orbit repeat (369 day, essentially a non-repeat orbit from the point of view of ocean and coastal dynamics). Moreover the available data only cover two non-sequential months. A different strategy must be attempted for the validation, which aims at exploiting the geographical spread of the full set of altimeter/Tide Gauge measurement pairs (match-ups), disregarding the time information.

We adopted the following methodology:

1. First of all we update some of the corrections in the Cryosat-2 data by fetching them from the state-of-the-art Radar Altimeter Database System (RADS). In detail, for each Cryosat-2 passfile we first find the corresponding RADS passfile and fetch (and interpolate to 20 Hz) a number of useful variables from there (ionospheric, tropospheric and geophysical corrections). We take from RADS also the distance from coastline
2. Then we compute the TWLE (total water level envelope) using those corrections. TWLE is the sea level inclusive of ocean tides and atmospheric forcing (due to pressure and wind effect), therefore immediately comparable with the level recorded by a tide gauge. TWLE is a desirable quantity for validation, as avoiding additional corrections by models of tides and atmospheric effect renders the validation results immune from errors in those models.
3. We finally subset all segments of each pass within 50 km from a tide gauge, and interpolate the tide gauge height (effectively a TWLE) on the time of the altimeter overpass

Figure 28 shows the locations of those segments of the Cryosat-2 passes in July 2012 and January 2013, which lay within 50 km from the Tide Gauges (black circles). We have attempted to correlate TWLE data over these multiple segments with the TG measurements from each corresponding gauge, also taking into account the distance of the altimetric measurements from the coastline.

Results of this multi-pass comparison are not satisfactory. There is a very large bias (order of a few m) in each altimeter/TG match-up. This bias varies depending on the particular matchup; its mean value is –725 cm, i.e. the altimeter TWLEs appear to be biased low w.r.t. the TG height by 725 cm. After removing this mean bias we have created 2-D

histograms of TWLE(alt)–TWLE(gauge), both as function of distance from TG and of distance from coast (Figure 29).

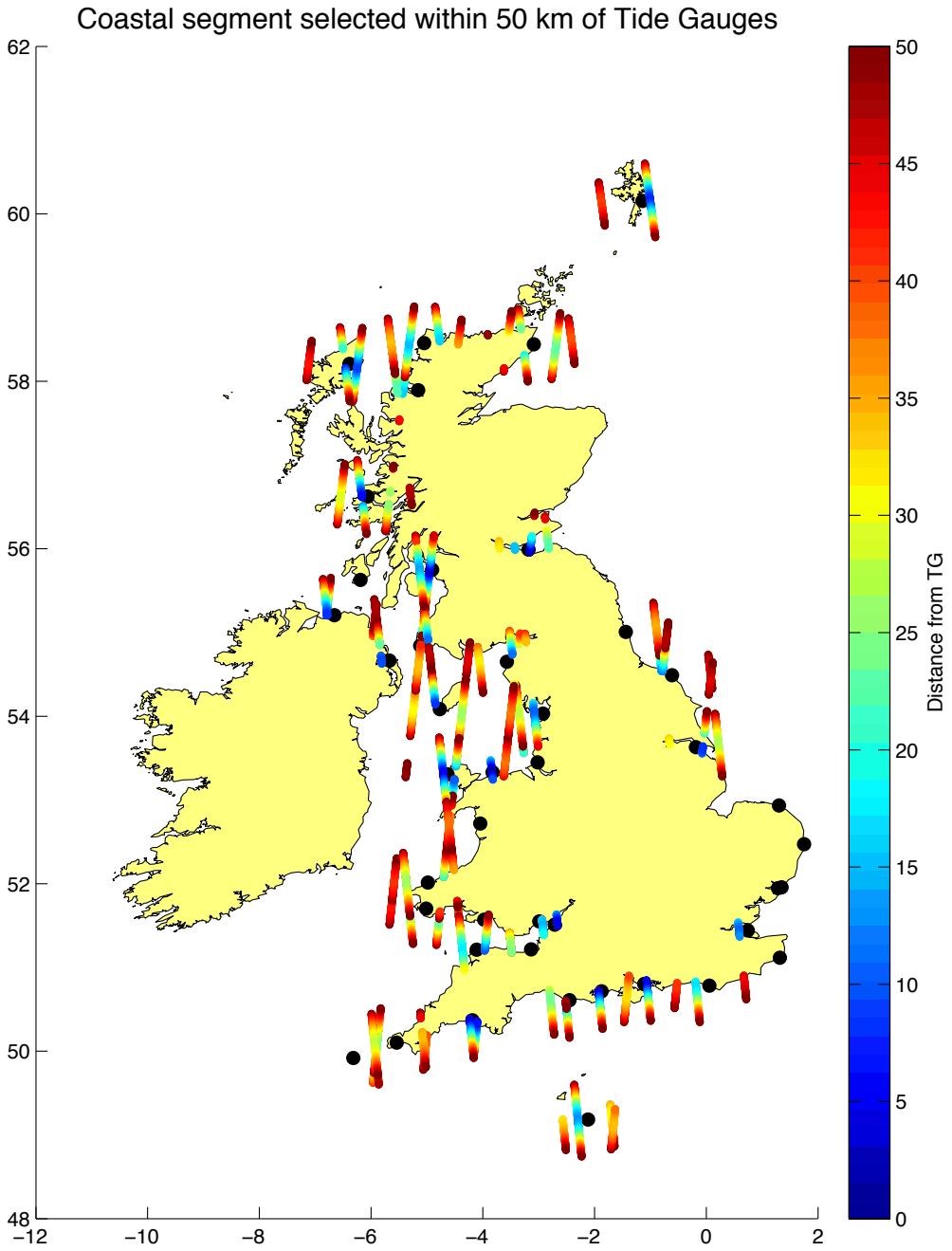

Figure 28: Segments of the Cryosat-2 passes in July 2012 and January 2013 around the UK coast located within 50 km from the Tide Gauges (black circles). The colour indicates distance from the closest gauge.

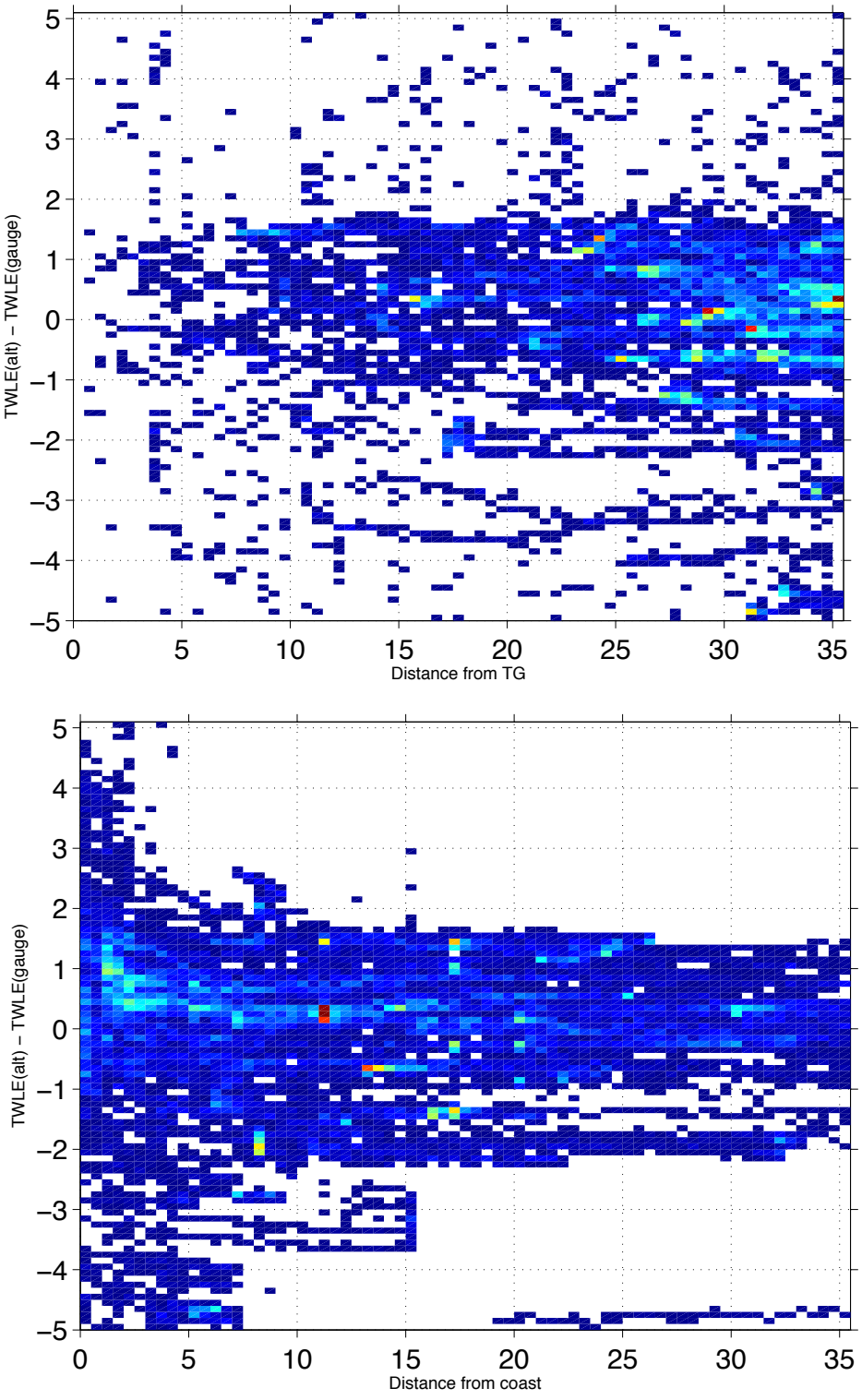

Figure 29: 2-d histograms of TWLE(alt)–TWLE(gauge), both as function of distance from TG (top) and of distance from coast (bottom)

We have then combined the information on TWLE difference (after mean bias removal), distance from the TG and distance from the coast in a single scatterplot ('spaghetti plot') shown in Figure 30 The large variations in TWLE difference (up to ±3 m) from pass to pass are apparent.

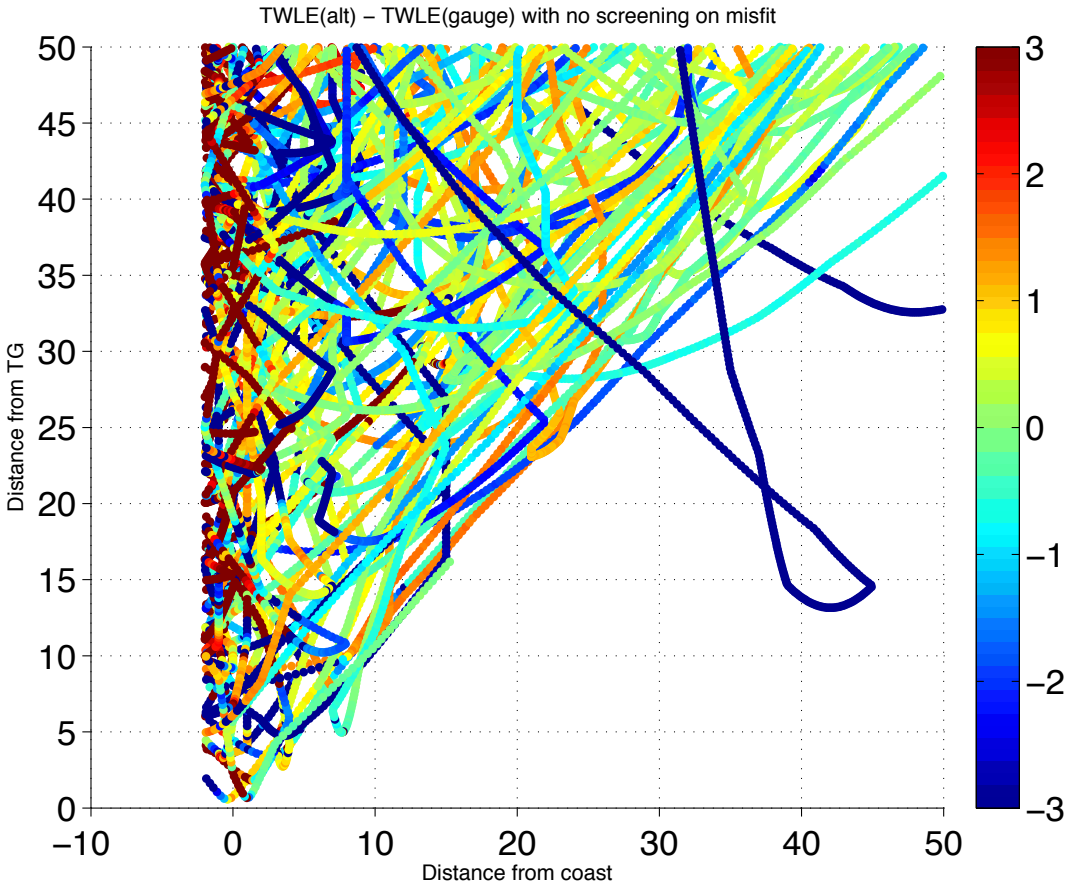

Figure 30: scatterplot of the (distance from coast, distance from TG) pairs along the track segments in Figure 28, color-coded according to the value of TWLE(alt)–TWLE(gauge).

We finally use the misfit parameter as defined in section 5.1 to screen the data, removing all the altimetric estimates for which misfit>3.5. The relevant plot is in Figure 31. This plot is also dominated by biases variable from match-up to match-up.

In order to confirm the presence of these large biases we also computed TWLEs from RADS (interpolated to 20 Hz, and after removing an overall mean bias to TG of –225 cm) and checked those TWLEs against the tide gauges. Figure 32 shows a scatterplot of the *(distance from coast, distance from TG*) pairs, color-coded according to the value of TWLE(RADS)–TWLE(gauge). The large biases variable from match-up to match-up are once again apparent and extremely similar to those in Figure 30 and Figure 31. A separate comparison of RADS and ESRIN TWLEs over an entire pass of those in Figure 1, shown in Figure 33, demonstrates that both datasets capture the same oceanographic features, but also highlights an unexplained mean bias of 450cm amongst them. We conclude that biases in Cryosat-2 test data for CP4O impact very negatively the validation and need further investigation.

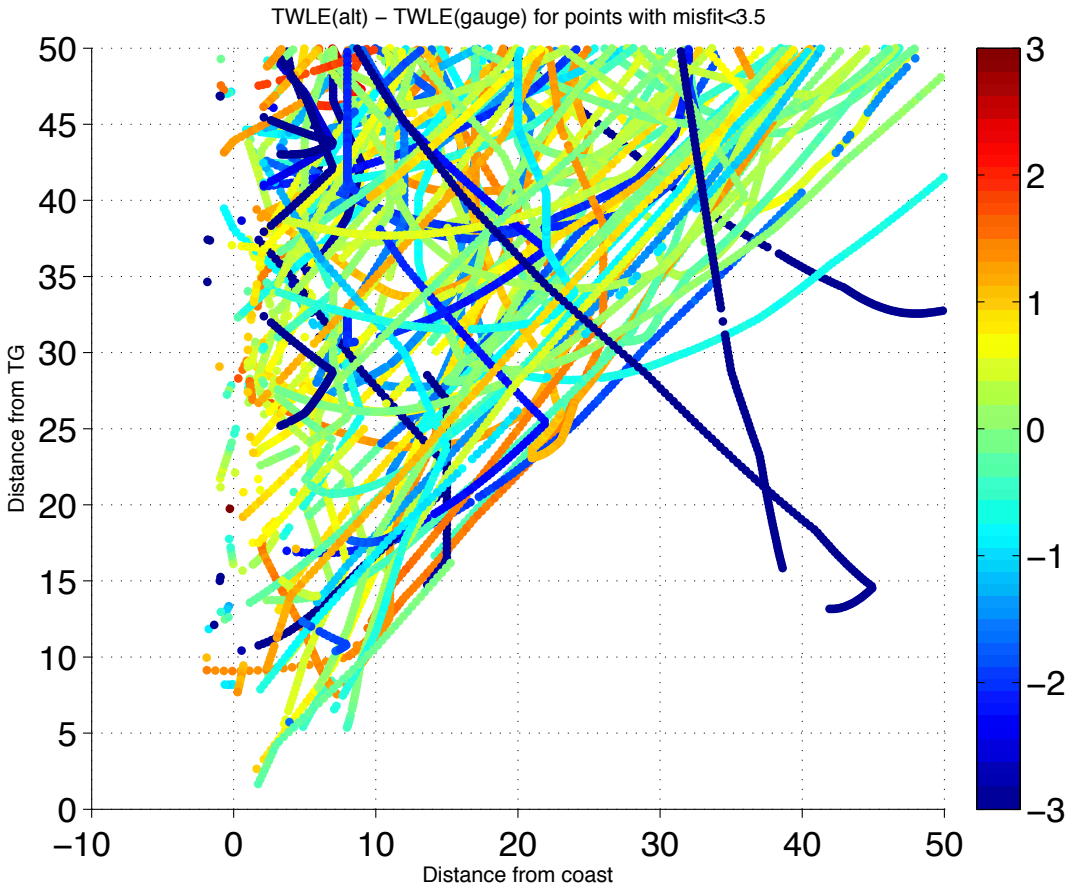

Figure 31: as in Figure 30, for points with misfit <3.5.

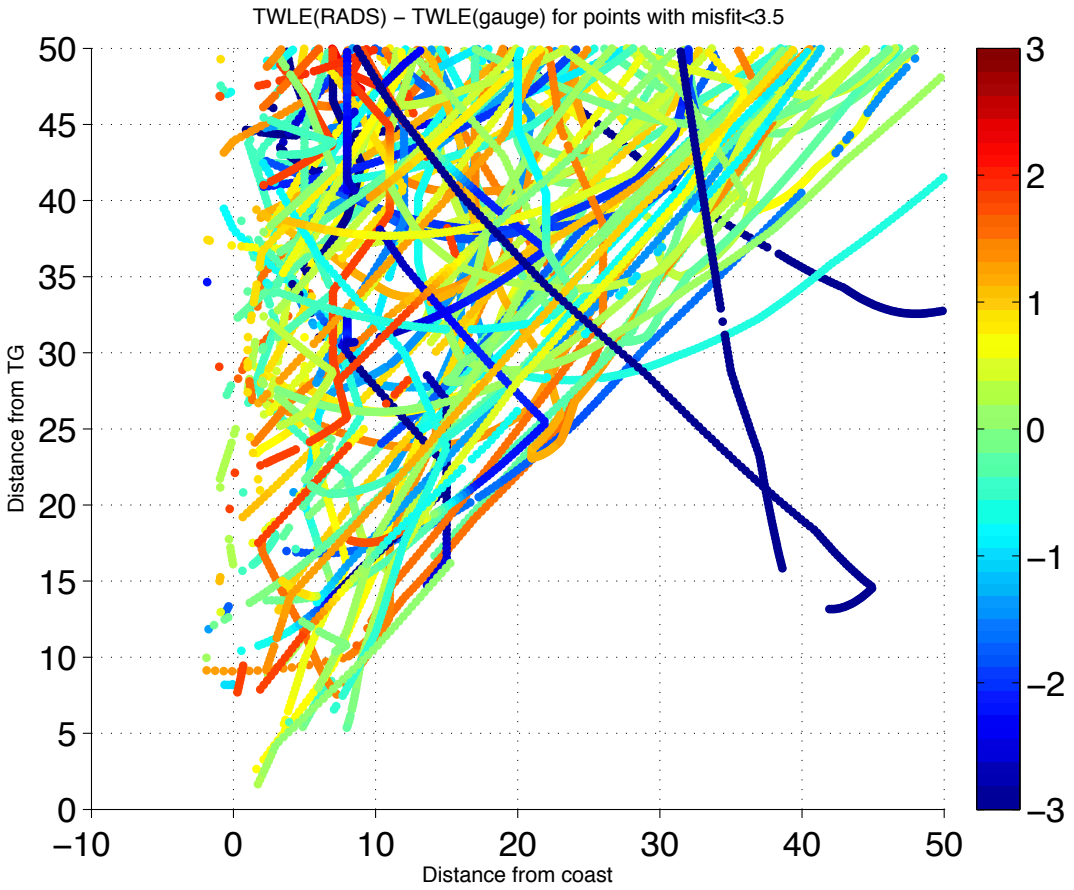

Figure 32: as in Figure 30, for points with misfit <3.5 (i.e. the same points as in Figure 31) but using TWLE computed from RADS (interpolated to 20Hz)

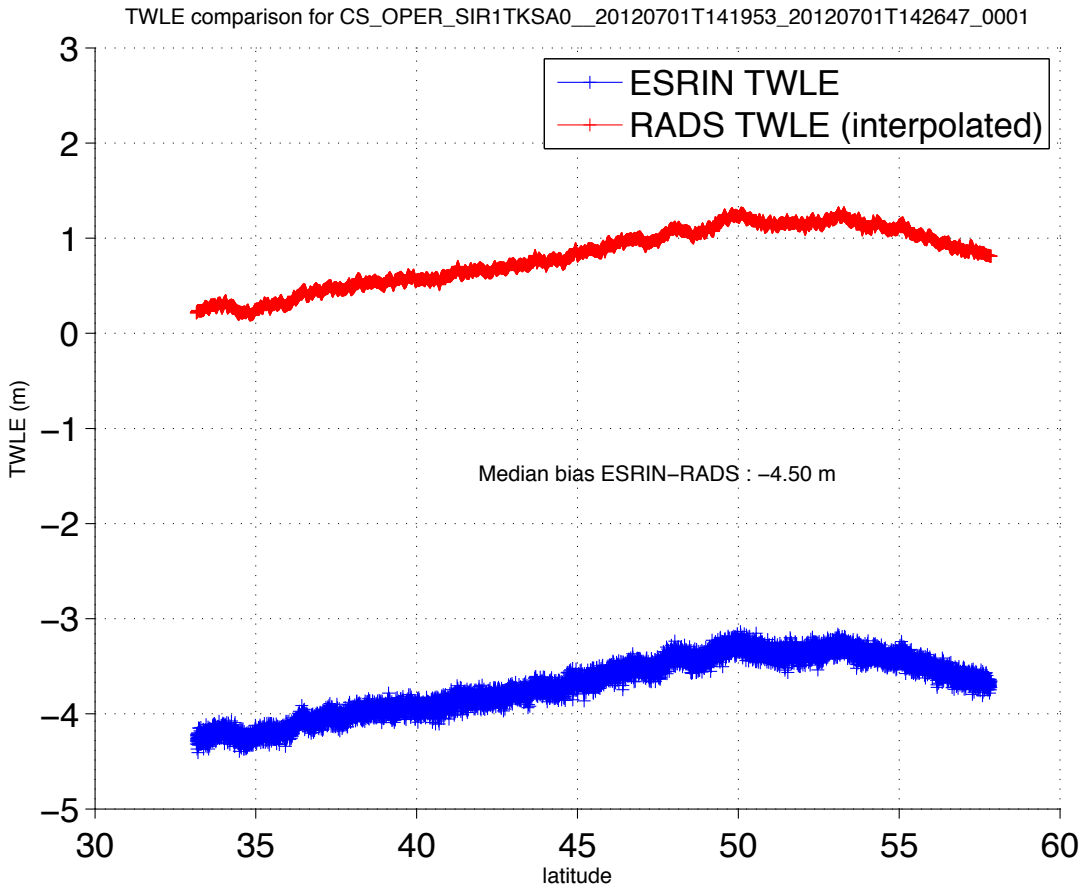

Figure 33: comparison of ESRIN TWLE and RADS TWLE over a longer pass segment

8.2 Additional verification of Cryosat-2 noise in the coastal zone

The unsatisfactory results in section 8.1 prompted us to carry out an independent verification of the noise level in 20-Hz Cryosat-2 TWLEs and its variation as a function of distance from coast. Therefore we selected the segments in all the tracks in Figure 1 that lay within 100 km of the UK coastline. For these segments we computed the 20-Hz TWLE as detailed in the previous section and then we computed the absolute value of difference between consecutive TWLE measurements, as already done in [RD5]. Given that between one 20-Hz measurement and the next the ground point will have moved just by ~300m, we expect the actual sea level to vary only by ~mm at most. Therefore the difference in measured sea level, which is normally of the order of a few cms, can be taken as a very good proxy of the measurement system noise. More precisely, assuming the noise to be gaussian with variance $\boldsymbol{\sigma}^2$, the difference amongst adjacent samples will have variance $2\boldsymbol{\sigma}^2$. The absolute value difference amongst consecutive TWLE measurements can therefore be used to estimate that noise and its variation as a function of distance from coast.

Shows the scatterplot of the absolute value of difference between consecutive TWLE measurements against distance from coast, and the statistics (median, 25th and 75th percentiles) of the distribution in 1-km-wide distance bins. Remarkably, the median

remains at ~5 cm up to 5Km from the coast, suggesting a noise level of ~3.5 cm for the 20-Hz data, which would correspond to 0.8 cm for the 1-Hz data. At 3 km the median abs(diff) is ~7.3 cm which would correspond to a noise level of 5.2 cm at 20 Hz.

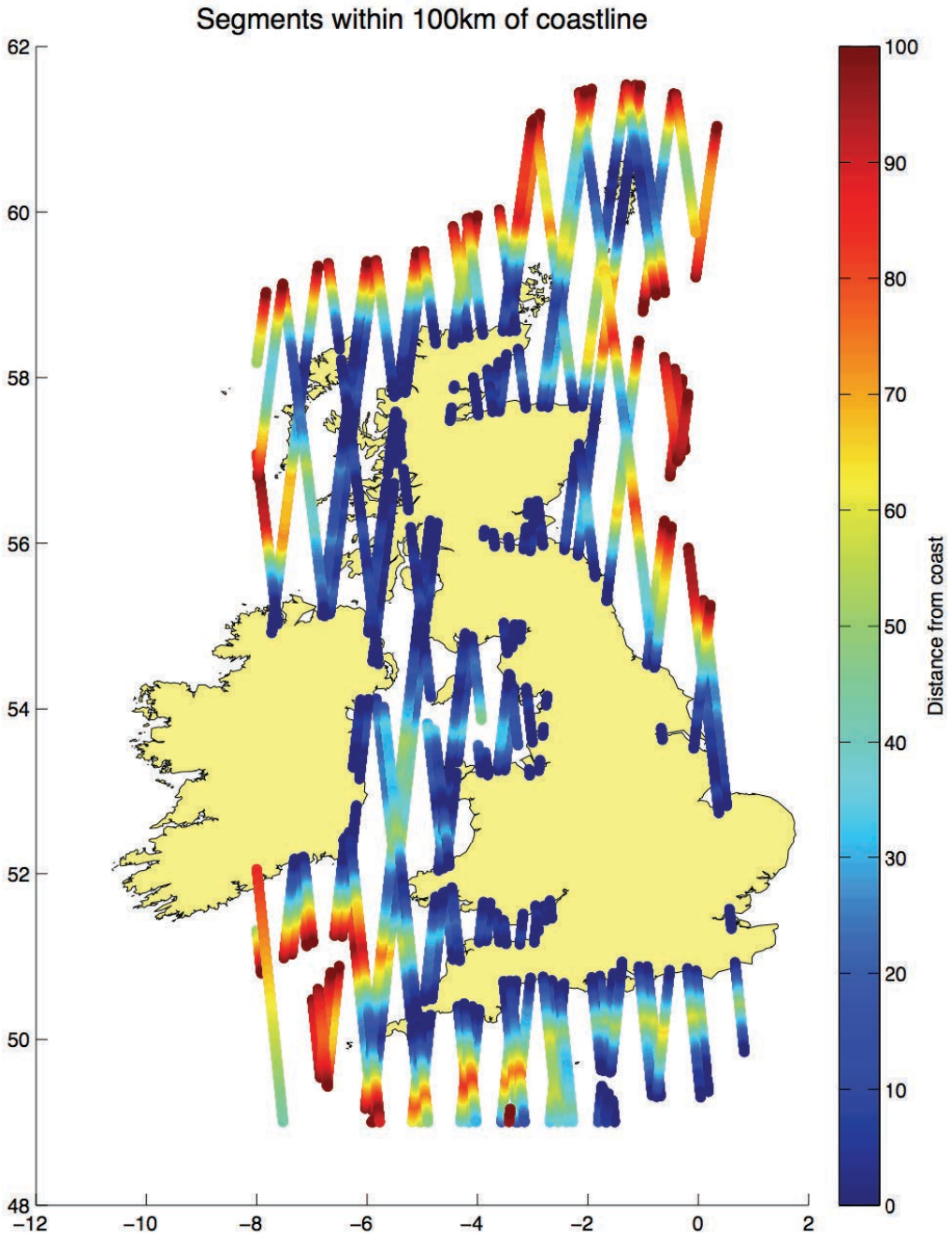

Figure 34: Segments of the Cryosat-2 passes in July 2012 and January 2013 within 100km of UK coastline, and their distance from the coast

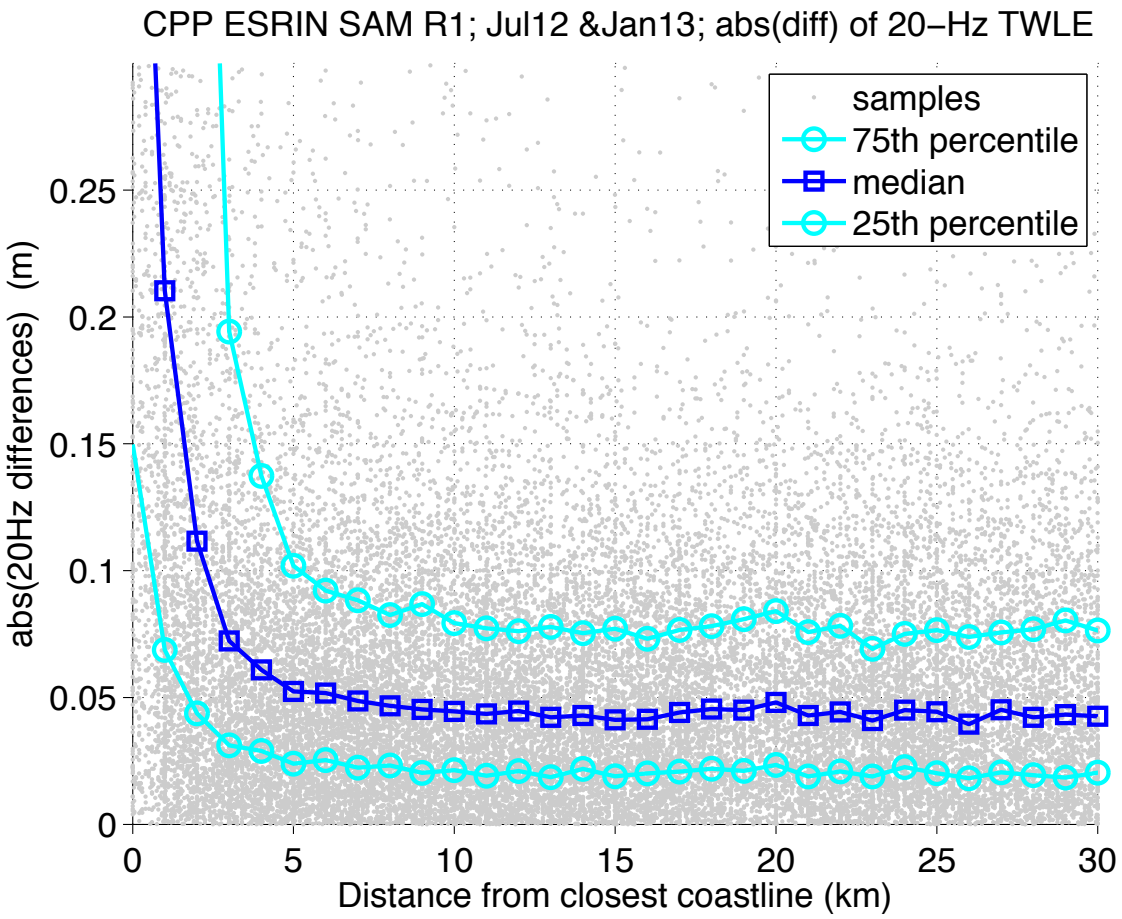

Figure 35: scatterplot of the absolute value difference between consecutive TWLE measurements against distance from coast, and the statistics of its distribution in 1-km distance bins

Finally we repeated the analysis of the absolute value of difference between consecutive TWLE measurements for only those points where the misfit is less than 3. The median stay virtually flat at ~5cm all the way to the coast (Figure 36), but obviously the fraction of points passing the misfit condition decreases quickly (it is about 60% at 5 km from the coast, and less than 25% at 3 km).. There is scope for setting 20-Hz precision targets in dependence on distance from the coast (for instance, one could require 8cm at 2km for one particular application) and finding the corresponding optimal misfit thresholds for the data screening

We note explicitly that in this exercise we have not examined the relative orientation of ground track and coastline, given the complexity of the UK coastline especially in its Northern and Western sectors, so the results in this section will be an average over the whole possible range of orientations. Nevertheless they demonstrate clearly that Cryosat-2 mantains an excellent performance of measurement well into in the coastal zone.

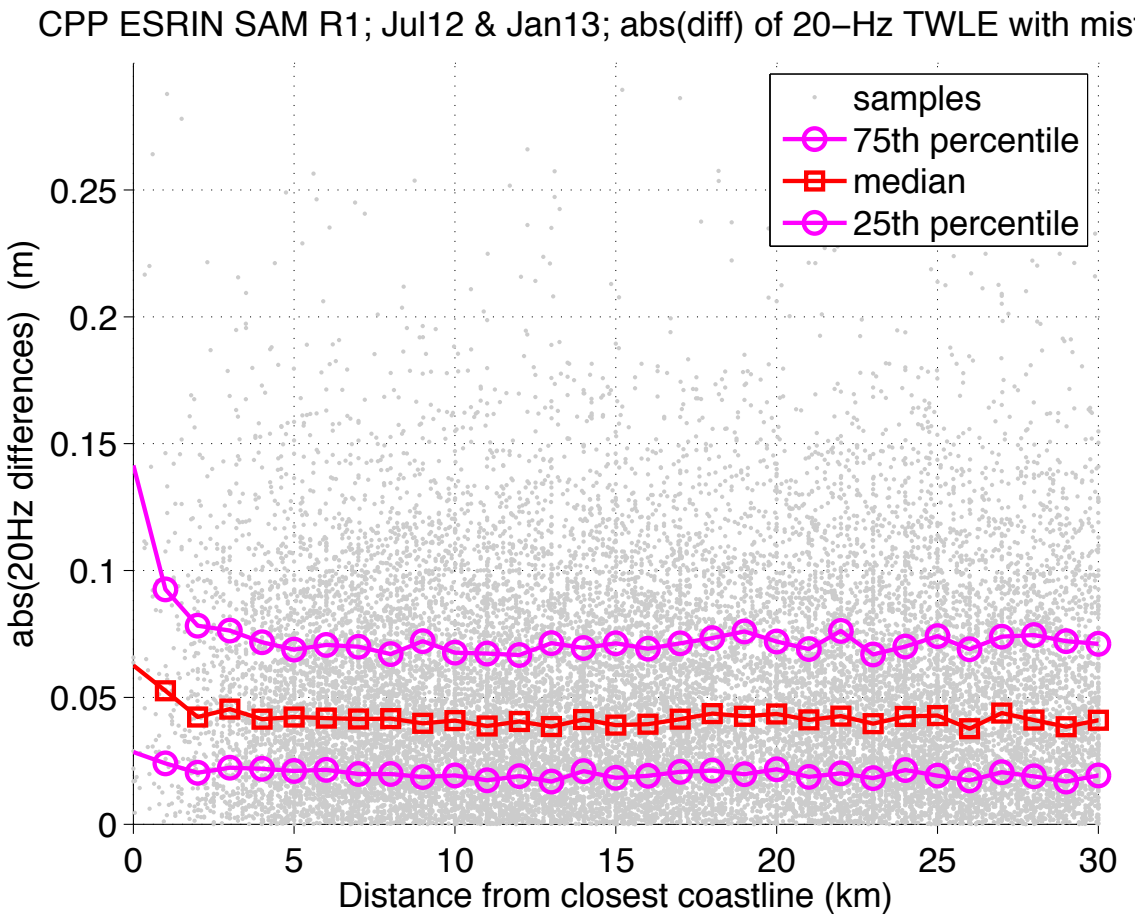

Figure 36: as in Figure 35, for those points with misfit <3

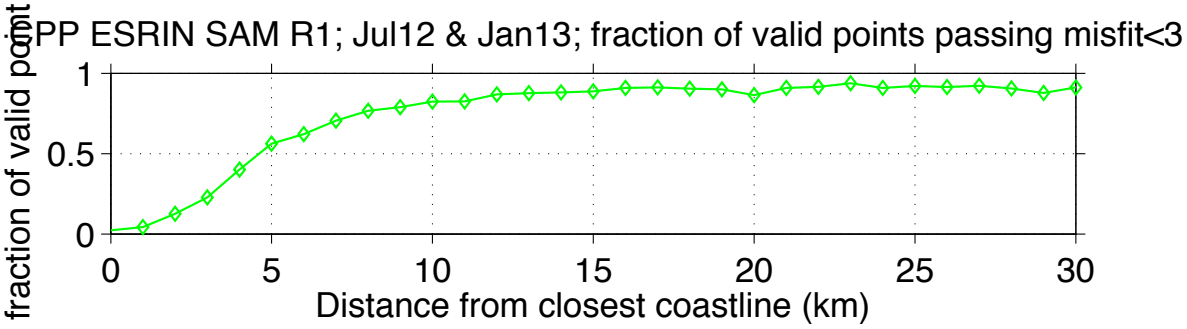

Figure 37: fraction of points with misfit <3 as a function of distance from coast

9 LIST OF ACRONYMS

C2	Cryosat-2
DDA	Delay-Doppler Altimetry
DDM	Delay-Doppler Map
GDR	Geophysical Data Record
J2	Jason-2
L1B	Level 1B
L2	Level 2
LRM	Low Rate Mode
ML	Multi-Look
S-3	Sentinel-3
SAR	Synthetic Aperture Radar
STM	Surface Topography Mission (on Sentinel-3)
SWH	Significant Wave Height (aka Hs or “wave height”)
TN	Technical Note
UKMO	UK Met Office
WP	Work Package